KfK 4898
August 1991

Review of Gyrotron Theory

E. Borie
Institut für Technische Physik

Kernforschungszentrum Karlsruhe

KERNFORSCHUNGSZENTRUM KARLSRUHE

Institut für Technische Physik

KfK 4898

Review of Gyrotron Theory

E. Borie

Kernforschungszentrum Karlsruhe GmbH, Karlsruhe

Als Manuskript gedruckt

Kernforschungszentrum Karlsruhe GmbH
Postfach 3640, 7500 Karlsruhe 1

ISSN 0303-4003

REVIEW OF GYROTRON THEORY

Abstract

This review gives a survey of the models used for the theoretical description of gyrotrons. After a brief phenomenological description of cyclotron resonance masers, in particular gyrotron oscillators, the computational methods used to calculate RF behavior in gyrotrons are described, with particular emphasis on those methods that have proved most useful for the calculation of the beam–field interaction in the resonator and for the practical design of gyrotrons at KfK.

THEORIE DES GYROTRONS

Zusammenfassung

Dieser Bericht gibt einen Überblick über die Modelle und Methoden, die für die theoretische Beschreibung eines Gyrotrons benützt werden. Nach einer kurzen phänomenologischen Beschreibung, werden die Rechenmethoden, die zur Beschreibung der Wechselwirkung zwischen Elektronenstrahl und Hochfrequenz (RF) Feld angewendet werden, diskutiert. Insbesondere werden die Methoden, die für die praktische Auslegung von Gyrotronen in KfK benutzt werden, beschrieben.

CONTENTS:

I. INTRODUCTION

It is not possible to provide a complete review of gyrotron theory in a single report of moderate length, since the literature is so extensive. This report will be limited to a brief phenomenological description of the cyclotron resonance and a review of the major models and computational methods used to study the beam–field interaction in the gyrotron resonator, as used for the analysis and design of gyrotrons. Excellent reviews of the early history of the gyrotron have been given by Flyagin et al (1977), Andronov et al (1978) and by Hirschfield and Granatstein (1977). Other important papers are given in the numerous special issues of the International Journal of Electronics (vol. 51, No. 4, Oct., 1981, vol. 53, No. 6, Dec. 1982, vol. 57, No. 6, Dec. 1984, vol. 61, No. 6, Dec., 1986, vol. 64, No. 1, Jan. 1988, vol. 65, No. 3, Sept. 1988) and the IEEE Transactions on Plasma Science (vol. PS–13, Dec. 1985, vol. PS–16, April 1988 and vol. PS–18, June 1990). In this connection the anthology "Gyrotrons: collected papers", USSR Academy of Sciences, Institute of Applied Physics, Gorki, 1981 and 1989 should also be mentioned. It will not be possible to discuss the results of the 1989 collected papers since a translation is not yet available. The subject of gyrotron theory has also been reviewed recently by Baird (1987).

This review will concentrate on computations of RF behavior in cylindrical gyrotrons. Some aspects of the theory are also valid for other types of gyrotrons. The main features of quasi–optical gyrotrons are well described in Sprangle et al (1981), Levush et al (1983), Bondeson et al (1983), Tran et al (1989), Fliflet et al (1990) and references therein.

Most practical examples will be taken from the KfK gyrotron program. However, we emphasize that the computational methods presented here are general, and the specific examples are used to illustrate general points.

GENERAL CHARACTERISTICS OF GYROTRONS

The gyrotron is a microwave power tube that emits coherent radiation at approximately the electron cyclotron frequency or its harmonics. Typical gyrotron oscillators are built as shown schematically in Fig. 1.1 A strong externally applied magnetic field supports the cyclotron motion of the electrons in the beam. The magnetic field in the interaction region is chosen such that the cyclotron frequency or one of its harmonics is close to the frequency of the RF field in the beam frame of reference. The interaction region consists of an open ended waveguide cavity, usually with a circular transverse cross section. The transverse components of the RF fields in this region interact with the electrons in the (usually) annular beam and convert the orbital kinetic energy into RF output. The electrons in the beam must therefore have a substantial transverse velocity $v_\perp$ as well as the usual

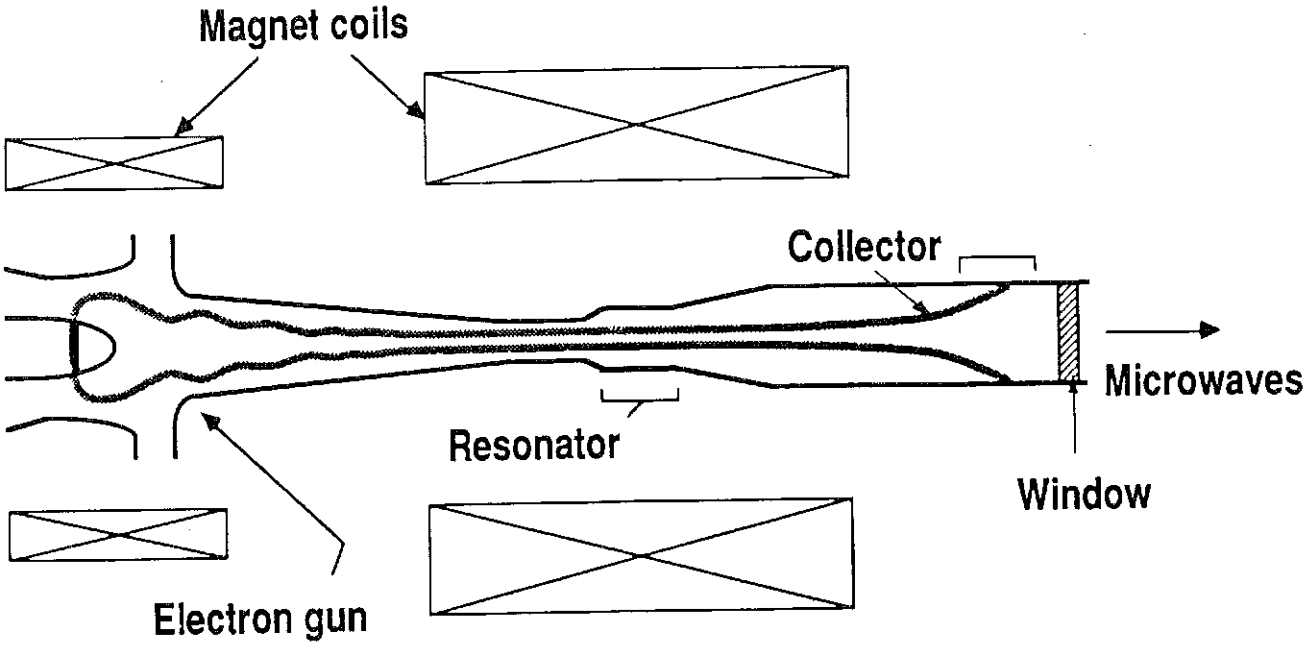

FIG. 1.1 Schematic diagram showing the longitudinal cross section of a typical gyrotron with the solenoids, MIG electron gun, RF interaction waveguide cavity, RF output waveguide and window.

longitudinal velocity v_z. Most of this transverse velocity comes as a result of the magnetic mirror effect produced by the increasing magnetic field leading to the interaction region. The final ratio of transverse to longitudinal velocity $\alpha = v_\perp / v_z$ in the interaction region is typically between 1 and 2 for gyrotrons that use magnetron injection guns with thermionic cathodes. The electrons follow helical paths around the lines of force of the external field. In order for a net flow of energy from the transverse electron motion to the electromagnetic wave to take place, the electrons must become bunched in phase within their cyclotron orbits. Such bunching can occur due to the fact that the electron cyclotron frequency

$$\omega_c = eB_0/m_e\gamma = \Omega_0/\gamma .$$

is a function of electron energy. Here e and m_e are the charge and rest mass of the electron, B_0 is the magnetic field in the resonator and $\gamma = E/m_e c^2$ is the usual relativistic factor. E is the total energy of the electron.

The phase bunching process can be most easily understood in the reference frame in which the axial electron velocity vanishes. In Fig. 1.2, an annular electron beam with radius R_e is depicted in this frame. The electrons arranged around this annulus execute circular orbits with radius $r_L = v_\perp \gamma/\Omega_0$. Typically $r_L << R_e$. Initially the phase of the electrons in their cyclotron orbits is random as shown. In the presence of a transverse RF electric field characteristic of a microwave cavity TE mode, the electrons will be accelerated or decelerated. As a specific example, Fig. 1.2 depicts an electric field with only an azimuthal component, as is characteristic of TE_{0n} modes in circular waveguides. With random phasing, there is no net energy exchange. Electron 1 will be decelerated by the azimuthal electric field and thus lose energy, while electron 2 will be accelerated and hence gain an equal amount of energy.

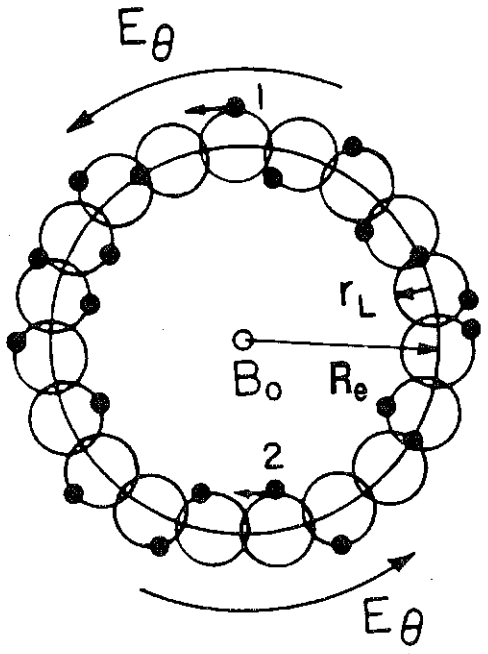

FIG. 1.2 Annular electron beam with initial random phasing of electrons in their cyclotron orbits.

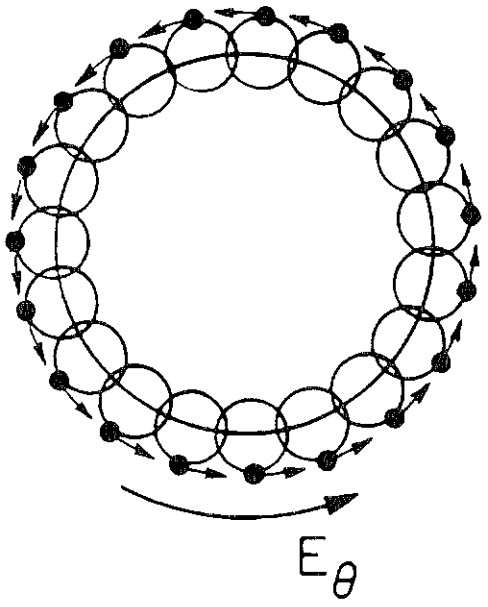

FIG. 1.3 Annular electron beam with electrons bunched in phase in their cyclotron orbits.

Phase bunching and net energy transfer can occur if the wave frequency is slightly larger than the initial value of the cyclotron frequency; that is, if

$$\omega' - eB_0/m_e\gamma_0' = (\delta\omega)' > 0.$$

where the subscript 0 denotes the initial value and the prime denotes the reference frame in which the electron axial velocity vanishes. Then, as electron 2 gains energy, its cyclotron frequency decreases; this electron falls farther from resonance, gaining less energy on each successive cycle. On the other hand, electron 1, which initially loses energy, experiences an increasing value of ω_c' and moves closer to exact resonance with the electric field, thereby losing an increasing amount of energy on each successive cycle. An instability develops in which the wave energy grows in time and the electrons bunch in phase within their cyclotron orbits as shown in Fig. 1.3. Once the electrons are bunched, they may give up energy to an electric field which reverses its direction in each half cycle of the cyclotron freqency in synchronism with the Larmor gyration of the electrons. This makes possible amplification of an electromagnetic wave at the electron cyclotron frequency. Other energy transfer mechanisms also play a role, as has been pointed out by Lindsay et al (1984), and actual

gyrotron performance is governed by a subtle interplay of these factors. Briefly, these are:

i. RF phase shift bunching due to the relativistic variation of the electron mass.

ii. Axial bunching due to the relativistic variation of the electron mass (if the RF magnetic field can be ignored and the external magnetic field is uniform, then γv_z and not v_z is constant. This shifts the gyrophase relative to a circularly polarized RF field).

iii. Antibunching counteracting both of these, due to the RF magnetic field. The effects are proportional to $1-c^2k_z^2/\omega^2$ and are thus small for TE modes near cutoff ($k_z \simeq 0$), as is usual for a gyrotron oscillator. They will be important in other devices, such as CARM's (cyclotron autoresonance maser), for which $k_z \neq 0$.

In terms of quantum theory, an electron in a magnetic field has a discrete energy spectrum for motion transverse to the magnetic field. According to Akhiezer and Berestetskii (1965), the energy levels (Landau levels) of an electron in a homogeneous magnetic field are given by

$$E_n^2/c^2 = m_e^2c^2 + p_z^2 + e\hbar B_0 (n-\mu+1/2) \quad \text{with } \mu=\pm 1.$$

The energy levels are unequally spaced, with $E_n-E_{n-1} > E_{n+1}-E_n$, and thus stimulated emission and absorption occur at slightly different frequencies. The condition $\omega' > \Omega\ \gamma'$ defines tuning the freqency of the RF field to correspond to stimulated emission of the transition $n \rightarrow n-1$. It has been pointed out by Flyagin et al (1977) that the bandwidth determined by the lifetime in a classical system is considerably larger than the frequency difference between the transitions $n \rightarrow n+1$ and $n \rightarrow n-1$, and this classical broadening completely dominates the interaction.

Two points should be mentioned briefly. Only the transverse energy of electron motion can be transferred to the RF field. This limits the efficiency. If we define $\alpha = v_\perp/v_z$, then the maximum efficiency which can be attained is

$$\eta_{max} \simeq \alpha^2/(1+\alpha^2).$$

It is thus desirable to work with a beam having as high a transverse energy as possible, consistent with limitations arising from reduced beam quality at higher values of α. Also, from the preceding, it is clear that $\omega > \omega_c$ if amplification is to take place, and that it is desirable to have the electrons give up their energy near the end of the interaction region. Otherwise, they may regain some of their energy from the RF field again. This is known as "overbunching."

In a microwave cavity, the operating frequency is determined by both the resonant freqency of the cavity mode and by the electron cyclotron frequency. Thus, the gyrotron can operate with improved stability in a higher order cavity mode as compared with other microwave tubes. Therefore gyrotron cavities are relatively large for a given operating

frequency and they can handle high power. A disadvantage of working with a large cavity is that the spectral density of cavity eigenmodes becomes large (the cavity is said to be overmoded) and mode competition can become a severe problem.

The electric field patterns for three major mode classes that have been used in gyrotrons are sketched in Fig. 1.4. The TE_{0n} modes with purely azimuthal electric fields have been employed in many gyrotrons (Gaponov et al (1975), Kreischer et al (1984a,b), Carmel et al (1982), Felch et al (1986)). However, gyrotrons designed to operate in simple TE_{0n} cavities have suffered from mode competition especially with TE_{2n} modes when $n \geq 3$ (Kreischer et al (1984a,b), Carmel et al (1982)). The "whispering gallery" TEmp modes with $m >> p$ (and $p=1,2$) have higher wall losses than the TE0n modes, but suffer less from mode competition, provided R_e is suitably chosen (typically on a radial maximum of the transverse field). Thus, such modes are promising candidates for high power gyrotrons operating at high frequencies. Asymmetric volume modes, with $m >> 1$ and $p > 2$ also show promise. They suffer less from high wall losses than whispering gallery modes. A typical example is also shown in Fig. 1.4.

The gyrotron development program at KfK concentrates on volume modes, either TE_{0p} or TE_{mp} with $p \geq 3$.

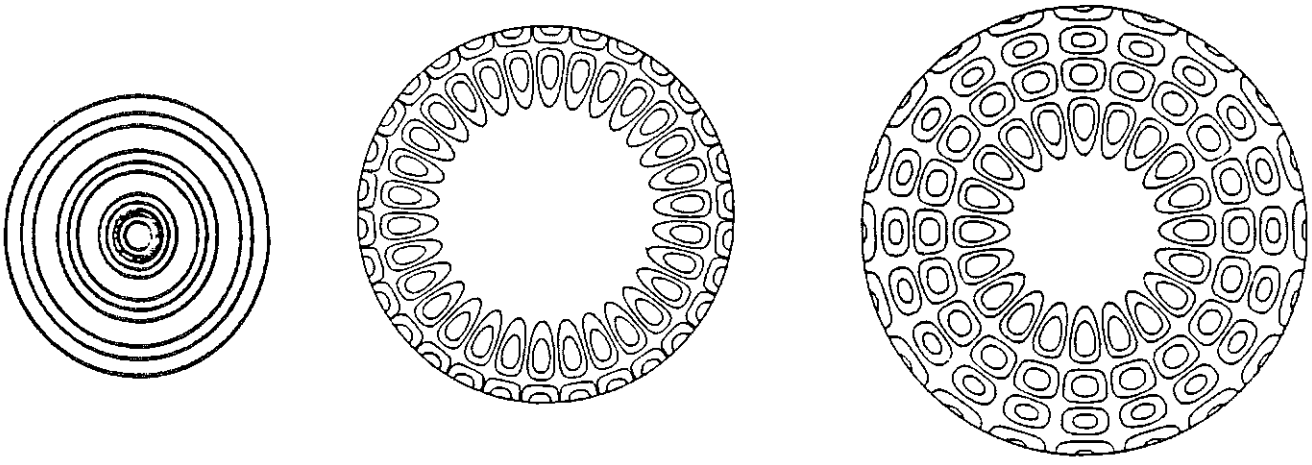

$TE_{0,3}$ $TE_{15,2}$ $TE_{10,4}$

FIG. 1.4 common classes of cavity modes used in gyrotrons.

II. ANALYSIS OF WAVEGUIDE CAVITIES

High power millimeter–wave gyrotrons require large overmoded waveguide cavities and transmission lines. The analysis of cavities for gyrotron applications is complicated by the fact that the open resonator must include arbitrary wall tapers and even steps. A number of generalized approaches have appeared in the literature (Bernstein et al, 1983, Luginsland 1985, Borie and Dumbrajs, 1985, Fliflet and Read 1981, Kuraev, 1979, Xu and Zhou, 1983, Derfler et al, 1982). The basic techniques are described in the books by Lewin (1975) and Sporleder and Unger (1979). This section will present in detail the method given by Borie and Dumbrajs. The other methods are equivalent.

The theory is based on the use of transverse field expansions in terms of orthonormal basis vectors, which, in turn, are derived from the wave potential functions used in TE and TM field analysis (see eg. Jackson, 1962). This type of basis vector expansion was introduced in 1951 by Marcuvitz as a technique for reducing Maxwell's equations in uniform waveguides to transmission line form. Such expansions of the transverse fields in terms of a complete set of orthonormal functions are, in fact, much more general.

The transverse HF electric and magnetic fields are assumed to have the time dependence $e^{i\omega t}$. The azimuthal dependence can be separated. Thus, the spatial dependence is assumed to be given by

$$\vec{E}(\vec{r}) = \Sigma\, \vec{e}_{mp}(r,z,\theta)\, V_{mp}(z) + \Sigma\, \tilde{e}_{mp}(r,z,\theta)\, U_{mp}(z) \qquad (1)$$

where

$$\int \vec{e}^{\,*}_{mp} \cdot \vec{e}_{m'q}\, dA = \delta_{mm}\ \delta_{pq}\,,$$

and similarly for the $\tilde{e}_{mp}$. The first sum in (1) corresponds to TE modes and the second sum to TM modes, so that the basis functions $\vec{e}_{mp}$ and $\tilde{e}_{mp}$ are given explicitly by

$$\vec{e}_{mp} \simeq \hat{z} \times \nabla\, \psi_{mp}\,, \qquad \tilde{e}_{mp} \simeq -\nabla_{\perp}\, \tilde{\psi}_{mp} \qquad (2)$$

with

$$\psi_{mp} = C_{mp}\, J_m(x_{mp} r/R(z))\, e^{-im\theta}\,,$$
$$\tilde{\psi}_{mp} = B_{mp}\, J_m(\gamma_{mp} r/R(z))\, e^{-im\theta}$$

Here $1/C^2_{mp} = \pi\,(x^2_{mp} - m^2)\, J^2_m(x_{mp})$ and $1/B_{mp} = \sqrt{\pi}\, y_{mp}\, J'_m(y_{mp})$.

are normalization constants, $k_{mp} = x_{mp}/R(z)$, $J'_m(x_{mp}) = 0$, $\gamma_{mp} = y_{mp}/R(z)$, and $J_m(y_{mp}) = 0$. This ensures that $E_\theta = 0$ at r=R(z), ie at the cavity wall. The HF magnetic field is obtained from $-\partial\vec{B}/\partial t = \nabla \times \vec{E}$. Thus

$$-i\,\omega B_z = -\Sigma\,\psi_{mp}\,k_{mp}^2\,V_{mp}(z)$$
$$-i\,\omega B_r = -\partial E_\theta/\partial z - im\,E_z/r$$
$$-i\,\omega B_\theta = \partial E_r/\partial z - \partial E_z/\partial r\,. \qquad (3)$$

When $m \neq 0$, E_z does not vanish. In order to satisfy the boundary conditions at the tapered cavity wall, it must satisfy the modified Bessel equation

$$-\nabla_\perp^2 E_z + \omega^2/c^2\,E_z - i\,\mu\omega\,J_z =$$
$$\Sigma\,\gamma_{mp}^2\,[\tilde{\psi}_{mp}\,dU_{mp}/dz - \frac{1}{R}\frac{dR}{dz}\,U_{mp}/r\;\partial(r^2\,\tilde{\psi}_{mp})/\partial r] \qquad (4)$$

and the boundary condition

$$E_z(R) = -\tan\theta_w\,E_r(R)$$
$$= -\frac{1}{R}\frac{dR}{dz}\,e^{-im\theta}\,\frac{1}{\sqrt{\pi}}\,\Sigma\,[\,im\,V_{mp}(z)\,/(x_{mp}^2 - m^2)^{1/2} + U_{mp}] \qquad (5)$$

One observes that it is impossible to satisfy the boundary condition at a tapered resonator wall with a pure TE mode when $m \neq 0$. In this case the TE and TM modes are coupled; the coupling is weak, however, for small taper angles and vanishes when m=0.

The functions $V_{mp}(z)$ and $U_{pm}(z)$ satisfy second order equations which are derived from

$$-i\,\omega\,\epsilon\mu\,E_r = \partial B_\theta/\partial z - im\,B_z/r + \mu J_r \qquad (6a)$$
$$-i\,\omega\,\epsilon\mu\,E_\theta = -\partial B_r/\partial z + \partial B_z/\partial r + \mu J_\theta\,. \qquad (6b)$$

One obtains, after multiplying (6a) by $(\vec{e}^{\,*}_{mq})_r$, (6b) by $(\vec{e}^{\,*}_{mq})_\theta$, adding and integrating over the transverse surface

$$d^2V_{mq}/dz^2 + (\omega^2/c^2 - k_{mq}^2(z))\,V_{mq} + \Sigma\,[2T^m_{qp}\,dV_{mp}/dz + dT^m_{qp}/dz\,V_{mp}]$$
$$-2R'/R\,\Sigma\,T^m_{pq}\,V_{mp} + (R'/R)^2\,V_{mq}\,[4m^2 - (x_{mq}^2 - m^2)^2]/3(x_{mq}^2 - m^2)$$
$$-2\,(R'/R)^2\,\Sigma\,x_{mp}^2\,V_{mp}/[(x_{mp}^2 - m^2)(x_{mq}^2 - m^2)]^{1/2}$$
$$\times\,\{[4x_{mp}^2\,x_{mq}^2 - 2m^2(x_{mq}^2 + x_{mp}^2)]/(x_{mq}^2 - x_{mp}^2)^2$$
$$+ m\,[1 - 4(x_{mq}^2 + x_{mp}^2)/(x_{mq}^2 - x_{mp}^2)][x_{mq} - x_{mp} - 1 - m(m+1)/x_{mq}x_{mp}]/(x_{mq} - x_{mp})\}$$
$$+ 2\,im/(x_{mq}^2 - m^2)^{1/2}\,\Sigma\,[\,2R'/R\,dU_{mp}/dz + (R'/R)'\,U_{mp}]$$
$$= +\,i\,\mu\omega\,J_{mq} \qquad (7a)$$

Similarly, one obtains, after multiplying (6a) by $(\tilde{e}^{*}_{mq})_r$, (6b) by $(\tilde{e}^{*}_{mq})_\theta$, adding and integrating

$$d^2U_{mq}/dz^2 + (\omega^2/c^2 - \gamma^2_{mq}(z))\, U_{mq} + \Sigma\,[2\tilde{T}^m_{qp} dU_{mp}/dz + d\tilde{T}^m_{qp}/dz\, U_{mp}]$$
$$-2R'/R\,\Sigma\,\tilde{T}^m_{qp}\,U_{mp} + (R'/R)^2\,U_{mq}\,[4 + y^2_{mq} - m^2]/3$$
$$+2\,(R'/R)^2\,\Sigma\,y^2_{mp}\,U_{mp}/(y^2_{mq} - y^2_{mp})^2\,\{\,2\,(y^2_{mq} + y^2_{mp}) -$$
$$-\,(m+1)(y_{mq} - y_{mp})/y_{mq}y_{mp}\,[y^2_{mq} - y^2_{mp} - 4(y^2_{mq} + y^2_{mp})/(y^2_{mq} - y^2_{mp})]\}$$
$$= +\,i\,\mu\omega\,\tilde{J}_{mq} \qquad (7b)$$

By definition, the mode coupling coefficients are

$$T^m_{pq} = 2\pi \int_0^R r\,\tilde{e}^{*}_{mq} \cdot \partial\tilde{e}_{mp}/\partial z\, dr$$

$$\tilde{T}^m_{pq} = 2\pi \int_0^R r\,\tilde{e}^{*}_{mq} \cdot \partial\tilde{e}_{mp}/\partial z\, dr \qquad (8)$$

Also

$$J_{mq} = \int d\theta \int_0^R r\,\tilde{e}^{*}_{mq} \cdot \vec{J}\, dr$$

$$\tilde{J}_{mq} = \int d\theta \int_0^R r\,\tilde{e}^{*}_{mq} \cdot \vec{J}\, dr\,. \qquad (9)$$

Straightforward integration gives, for TE modes

$$T^m_{pq} = -\frac{2}{R}\frac{dR}{dz}\,[(x^2_{mp} - m^2)/(x^2_{mq} - m^2)]^{1/2}\, x^2_{mq}/(x^2_{mp} - x^2_{mq}) \qquad p \neq q$$

$$T^m_{qq} = -\frac{1}{R}\frac{dR}{dz}\, m^2/(x^2_{mq} - m^2)$$

and

$$\tilde{T}^m_{pq} = +\frac{2}{R}\frac{dR}{dz}\, y^2_{mp}/(y^2_{mq} - y^2_{mp}) \qquad p \neq q$$
$$\tilde{T}^m_{qq} = -\frac{1}{R}\frac{dR}{dz}$$

for TM modes. The coupling between the TE and TM modes is given explicitly in (7).

In general, one wishes to minimize reflections at the resonator output. In this case, we require

$$\partial\vec{E}/\partial z = -ik_z\vec{E} \qquad \text{and} \qquad \partial\vec{B}/\partial z = -ik_z\vec{B}$$

at the resonator output end, $z = z_{out}$ (see Fig. 2.1).

When a source is present, the eigenfrequency of a steady state solution is real, in contrast to the cold cavity case, in which the eigenfrequency has a positive imaginary part to account for damping due to radiation out of the cavity. In that case, the normalization of the field profile is determined by the source term. The cold cavity fields can be normalized to the desired output power as follows: Poynting's theorem gives

$$P_{out} = \pi \int_0^R r\, dr\, Re(\vec{E} \times \vec{H}^*)_z|_{z=z_{out}} \qquad (10)$$

Inserting explicit expressions for the fields and using the radiation boundary condition gives finally

$$\begin{aligned} P_{out} = Re\,(1/2\,\mu\omega) \Big[& \sum_p (k^*_{zmp} |V_{mp}|^2 + \gamma^*_{zmp} |U_{mp}|^2) \\ & -i \sum_{pq} (V^*_{mq} T^m_{qp} V_{mp} + U^*_{mq} \tilde{T}^m_{qp} U_{mp}) \\ & + \sum_{pq} 2m\, R'/R\, (x^2_{mp} - m^2)^{-1/2} V_{mp} U^*_{mq} \\ & -2\pi i \sum_p \gamma^2_{mp} U_{mp} \int_0^R r\, \tilde{\psi}_{mp} E^*_z\, dr \Big] \end{aligned} \qquad (11)$$

Use of the generalized telegrapher's equations (Schelkunoff, 1952, 1955, Sporleder and Unger, 1974) will give equivalent results. This approach has been used by, among others, Fliflet and Read (1981). At least to first order in the mode coupling coefficients, the equations are equivalent. Direct use of a second order equation seems to be easier to carry out in practice. The method presented here is identical to that given by Luginsland (1985) for the case of azimuthally symmetric modes and moderate taper angles, and similar to that given by Kuraev (1979) and Bernstein et al (1983). These authors use a slightly different Ansatz for the basis functions which results in minor differences in the equations.

This formalism is valid when R(z) is continuous and differentiable. If the cavity profile R(z) has discontinuities, it is necessary to solve the equations piecewise, and match the fields and their derivatives at the discontinuities of R(z). This will be illustrated in the section on complex cavities.

The functions $V_{mp}(z)$ must also satisfy radiation boundary conditions at the ends of the resonator (Bratman et al 1981a):

$$dV/dz|_{z_{in}} = ik_z(z_{in})\, V(z_{in}) \quad \text{and} \quad dV/dz|_{z_{out}} = -ik_z(z_{out})\, V(z_{out}) \qquad (12)$$

The meaning of z_{in} and z_{out} is explained in Fig. 2.1, which shows the resonator geometry considered in this work.

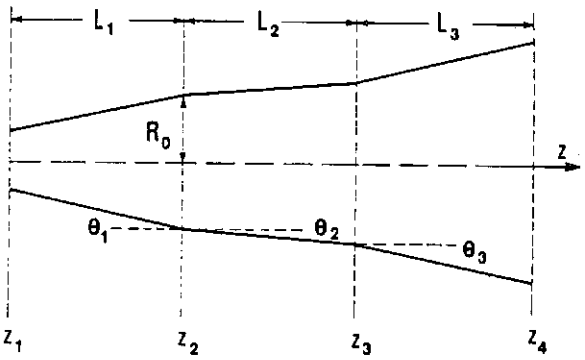

FIG. 2.1 Resonator geometry. $z_{in}=z_1$ and $z_{out}=z_4$. Most of the first section is below cutoff to ensure that no RF power can reach the gun. The second section is also called the midsection, and the third section permits the RF output to leave the resonator.

For numerical calculations, the boundary condition at z_{in} is used to determine the starting value of dV/dz for the integration of (7a,b) and the boundary condition at z_{out} is reformulated in the form

$$|R| = |(dV/dz + ik_z V)/(dV/dz - ik_z V)| = \text{minimum.}$$

One could also specify a nonzero reflection coefficient R_{load}, in which case, the condition $|R-R_{load}|$ = minimum is imposed.

In the codes used at KfK, the minimization of $|R|^2$ as a function of frequency ω and Q (in cold cavity approximation) is done with the CERN subroutine MINUIT (James and Roos, 1974). For the coupled equations (7), a standard Runge–Kutta routine is used. To be sure that the oscillatory behavior of the RF field in the region of the output is reproduced accurately, a stepwidth $\Delta z \simeq \lambda/20$ is sufficicent. Whatever numerical method is used to integrate the equations, accuracy will be poor if $\Delta z > \lambda/10$. For a further discussion of the effect of stepwidth in integrating the equation of motion for a harmonic oscillator, see Sect. 4.6 of Hockney and Eastwood (1981).

As an example, Fig. 2.2 shows the result of a typical calculation for a mode with $m \neq 0$, in this case the $TE_{10,4}$ mode. The resonator is a design candidate for an experiment at KfK. With the notation given in Fig. 2.1, we have $\theta_1 = 5^\circ$, $L_1 = 10$ mm, $\theta_2 = 0^\circ$, $L_2 = 11$ mm, $\theta_3 = 3^\circ$, and $L_3 = 12$ mm. The cavity radius is 8.11 mm and the resonant frequency and quality factor are 140.124 GHz and 663, respectively. Note that for the small taper angles considered here, there is very little mixing with the $TE_{10,3}$, $TE_{10,2}$ and $TM_{10,3}$ modes.

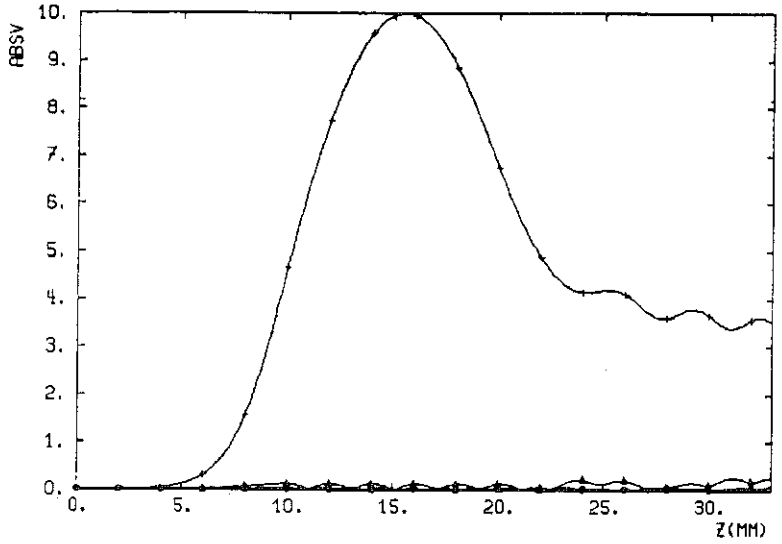

FIG. 2.2 Field profiles for the TE10,4 mode, including mixing with the TE10,3, TE10,2 and TM10,3 modes due to the resonator tapers. The oscillations indicate exchange of energy among the various modes. Resonator geometry is described in the text.

Mixing to other modes ($TE_{10,1}$, $TM_{10,1}$, $TM_{10,2}$, $TM_{10,4}$) is even smaller. For such parameters, it is completely legitimate to use the Vlasov approximation widely considered in the literature, in which only a single TE_{mp} mode is retained in the expansion (1) and coupling to other modes due to the cavity taper is neglected. Differences do not start to become noticeable until the taper angle exceeds about 6°. In the single mode approximation, we then have

$$d^2V_{mq}/dz^2 + (\omega^2/c^2 - k_{mq}^2(z))\, V_{mq} \simeq i\omega J_{mq} \,. \qquad (13)$$

The solution of the simplified equation (13) is best carried out with the Numerov algorithm (Scheid, 1968). For the example just described, the resonant frequency and quality factor obtained with the simplified equation are 140.128 GHz and 590, respectively.

It is instructive to examine the dependence of frequency and quality factor on the resonator geometry. Some results have been presented by Borie et al 1986, 1988, as well as by Barroso et al 1986 (this list does not pretend to be exhaustive). Here, as an example, we examine the dependence of frequency, quality factor and field profile on θ_1, L_2 and θ_2 for gyrotrons relevant for the KfK development program. The qualitative trends are clearly applicable to other cases. The output taper angle θ_3 was fixed at 3°, and $L_3 \simeq$ 11 mm. The cavity radius is about 3.47 mm, corresponding to a TE_{03} mode oscillating at 140 GHz, or 3.24 mm, corresponding to a TE_{03} mode oscillating at 150 GHz. Fig. 2.3 shows field profiles for a resonator having $L_2 =$ 10 mm for various values of θ_1 and θ_2. The effective length and

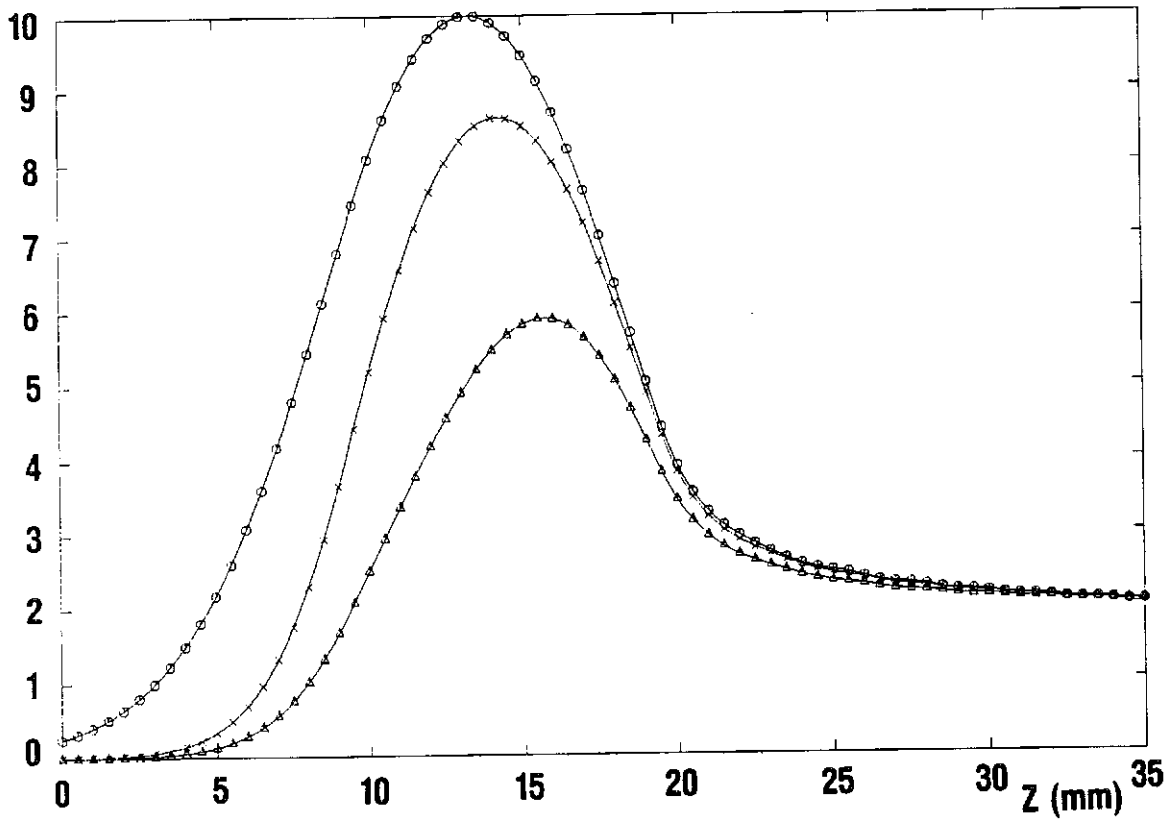

FIG. 2.3 Field profiles for the TE03 mode, ignoring mixing due to resonator tapers. Here R_0=3.24 mm, L_1= 10 mm, L_2= 10 mm, θ_3= 3°, L_3= 15 mm

circles: θ_1= 0.25°, θ_2= 0°, F= 150.02 GHz, Q=1195 .

crosses: θ_1= 1 °, θ_2= 0°, F= 150.09 GHz, Q=807.

triangles: θ_1= 1 °, θ_2= 0.1°, F= 149.83 GHz, Q=411.

quality factor are influenced by the input taper. When θ_1= 1/4°, the field profile extends into the input section and the quality factor goes up, in comparison to the case with θ_1= 1°. When $\theta_2 \neq$ 0°, the maximum of the field profile is pushed toward the end of the resonator, and the field profile is asymmetric. The effective length, given approximately by the full width at half maximum, is not much different from the case when θ_2= 0°; however, the resonator is a little further from cutoff at the start of the output taper, resulting in a lower wave impedance at that point and a considerable reduction in quality factor. Also note that the TE_{031} mode is slightly below cutoff in part of a tapered mid section. This results in a

smaller difference in resonant frequency and quality factor as compared with the TE_{032} mode, as seen in Table 1. Field profiles for the neighboring TE_{231} and TE_{521} modes are nearly identical to those of the TE_{031} mode for the same geometry. Table 1 and Fig 2.4 illustrate the comparison of the TE_{03} modes with different axial indices for resonator geometries considered for use at KfK in the experiments at 140 GHz. When $\theta_2 = 0^\circ$, the quality factor of the TE_{032} mode is nearly a factor of 4 smaller than that of the TE_{031} mode, while the corresponding factor is 2 or less for the tapered mid section with $\theta_2 = 0.1^\circ$. The frequency differences between the modes with larger axial index is smaller for the longer resonators, as expected.

Table 1 : Frequency, quality factor and (for n=1) full width at half maximum for the TE03n modes as a function of resonator geometry. The value of θ_3 is fixed at about 3° and $L_3 \simeq 11$ mm.

n	L_1(mm)	$\theta_1(^\circ)$	L_2(mm)	$\theta_2(^\circ)$	F(GHz)	Q	L_{fwhm}(mm)
1	18.9	0.5	10	0	140.23	851	11.0
2					141.16	257	
1	18.9	0.5	10	0.1	139.95	424	11.0
2					140.95	206	
1	13	1	15	0	140.50	1679	13.4
2					141.13	432	
1	13	1	15	0.1	139.96	481	13.4
2					140.70	298	

It is often convenient to work with a normalized field profile. This will be defined by

$$V_{mp}(z) = V_{max}\, \hat{f}_{mp}(z)\,. \qquad (14)$$

Here, $\hat{f}_{mp}(z)$ is the field profile normalized to a maximum absolute value 1. In the cold cavity approximation, V_{max} and the output power are related by :

$$Q\, P_{out} = \omega\, W = \omega\, \epsilon_0/2\, V_{max}^2 \int_{z_{in}}^{z_{out}} |\hat{f}_{mp}(z)|^2\, dz. \qquad (15)$$

It is also instructive to examine the phase of the field profile. Fig 2.5 does this for the untapered 10 mm resonator also discussed above. Here the amplitude and phase (mod 2π) of the normalized field profile $\hat{f}(z)$ are given for the TE_{031} and TE_{032} modes. The phase of

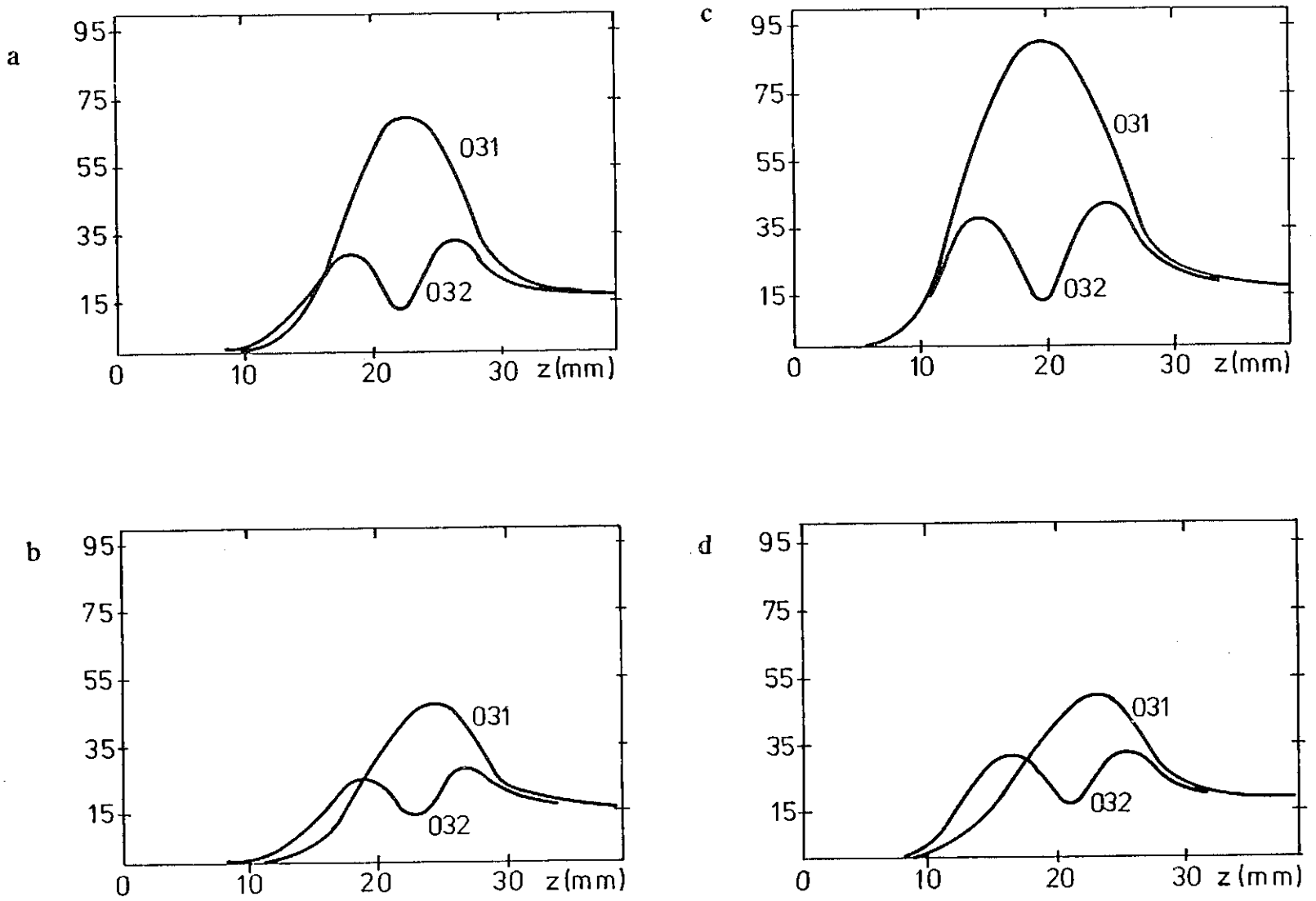

FIG. 2.4 Field profiles for the TE031 and TE032 modes for various resonator geometries.

a) $\theta_2 = 0^\circ$, $L_2 = 10$ mm b) $\theta_2 = 0.1^\circ$, $L_2 = 10$ mm

c) $\theta_2 = 0^\circ$, $L_2 = 15$ mm d) $\theta_2 = 0.1^\circ$, $L_2 = 15$ mm

the TE_{031} mode remains nearly constant at zero until shortly after the magnitude has reached its maximum; the decrease is approximately linear for z>about 32 mm, which corresponds to 2λ after the start of the tapered third section. This behavior is typical. The phase of the TE_{032} mode goes through $-\pi$ at the minimum of $|\hat{f}(z)|$ and becomes linear (corresponding to an outgoing plane wave) at distances about 3λ from the start of the third section. When modeling the RF behavior, it is important to treat the region in which the field profile is large correctly. This includes not only the resonator mid–section, but also

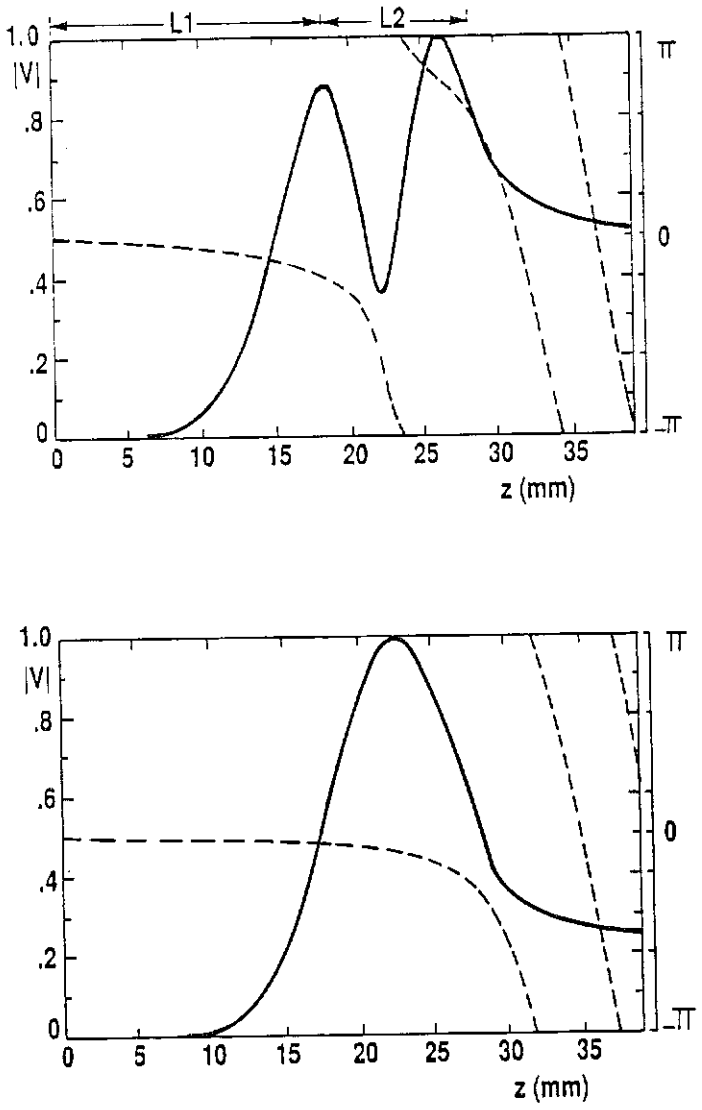

FIG. 2.5 Amplitude and phase (mod 2π) of normalized field profiles for the TE031 and TE032 modes for the resonator geometry R_0=3.47 mm, θ_2= 0°, L_2= 10 mm.

parts of the input and output tapered sections, corresponding to distances of about 2–3 λ on each side of the mid–section. An exact treatment of the remainder of the resonator is less important. As will be discussed below, this is also the region in which significant interaction with the electron beam also takes place.

The type of analysis presented here seems to work better for highly overmoded gyrotron resonators than the mesh methods of cavity analysis often used in accelerator physics (see, eg., Weiland, 1984). Such programs usually assume closed cavities. Also, numerical stability requires that the mesh intervals Δr and Δz be comparable in size. For gyrotron resonators, one requires $\Delta r/R_0 < 1/2\pi p$ (R_0 is the radius of the resonator, p is the radial index of the mode of interest). R_0 is determined by $2\pi/\lambda \simeq x_{mp}/R_0$. Typically, $\Delta z \simeq \lambda/20$ suffices for accuracy, but one must take the much smaller value $\lambda/4\pi^2 p x_{mp}$, which increases the memory requirements drastically. In addition, the resonant frequency is approximately equal to $[f_c^2+n^2/4L^2]^{1/2}$ where L is the length of the resonator and n=1,2,3,... is the axial index. $f_c = cx_{mp}/2\pi R_0$. For TE modes close to cutoff, the closely spaced resonant frequencies calculated by such programs correspond to different axial indices and the same radial index, which is difficult to control without special programming tricks. For such cases, the expansions described here are easier to work with.

III. EQUATION OF MOTION

In the absence of an RF field (but in the presence of a nearly uniform magnetic field B_0 in the z–direction), the electrons gyrate about the guiding center at the cyclotron frequency

$$\omega_c = eB_0/m_e\,\gamma = \Omega_0/\gamma\,.$$

The gyration radius is given by $r_L = u_t c/\Omega_0$. Here u_t is the component of $\vec{u} = \gamma\vec{v}/c = \gamma\vec{\beta} = \vec{p}/m_e c$ perpendicular to the external magnetic field. It is convenient to treat the unperturbed (by the RF field) motion quasi–analytically. This leads either to a slow variables transformation (Rapaport et al 1967 or Ganguly and Ahn 1982) or, with the further approximation of neglecting the RF magnetic fields and guiding center drift, to the so–called "adiabatic" approximation (Fliflet et al, 1982, Bratman et al, 1973, Mourier, 1980). If

$\Psi = \int_{t_0}^{t} \Omega_0/\gamma\,dt + \phi - \phi_0$, we make the Ansatz

$$u_x + i\,u_y = i\,u_t\,e^{i\Psi} \qquad \text{and thus}$$

$$x = X_0 + r_L\cos\Psi\ ,\ y = Y_0 + r_L\sin\Psi\,.$$

$X_0 = R_e\cos\theta_e$ and $Y_0 = R_e\sin\theta_e$ define the position of the electron's guiding center. (see Fig. 3.1) In the absence of an RF field, this provides an exact solution of the equations of motion, with the electrons gyrating around the fixed (for uniform magnetic fields) guiding center (X_0, Y_0).

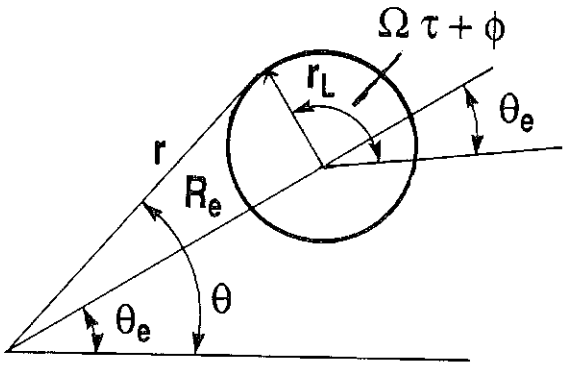

FIG 3.1: Projection of an electron orbit in the transverse plane, showing the various orbital parameters.

To describe the interaction with the RF field, we define $\vec{a} = -e/m_e c\,(\vec{E}_{RF} + \vec{v} \times \vec{B}_{RF})$. After some manipulation (work out the components of $d\vec{u}/dt = \vec{a} - e/m_e c\,\vec{v} \times \vec{B}_0$, take appropriate linear combinations for the transverse variables and transform to cylindrical polar coordinates) one obtains the system of slow variables equations, with $\eta = e/m_e c$:

$$du_t/dt = a_r \sin(\theta-\Psi) + a_\theta \cos(\theta-\Psi) + \eta c u_z/2\gamma\,(r_L + R_e \cos(\Psi-\theta_e))\, dB_0/dz$$

$$u_t\, d\phi/dt = a_\theta \sin(\theta-\Psi) - a_r \cos(\theta-\Psi) - \eta c u_z/2\gamma\, R_e \sin(\Psi-\theta_e)\, dB_0/dz$$

$$dz/dt = c\, u_z/\gamma$$

$$du_z/dt = a_z - \eta c u_t/2\gamma\,(r_L + R_e \cos(\Psi-\theta_e))\, dB_0/dz$$

$$\Omega_0/c\, dR_e/dt = -a_\theta \cos(\theta-\theta_e) - a_r \sin(\theta-\theta_e) - \eta c u_z/2\gamma\, R_e\, dB_0/dz$$

$$\Omega_0/c\, R_e\, d\theta_e/dt = -a_\theta \sin(\theta-\theta_e) + a_r \cos(\theta-\theta_e) \qquad (16)$$

This form of the equation of motion has been used to test the accuracy of the "adiabatic" equation to be discussed below. An example for the case of starting currents is given by Borie and Jödicke (1988). It was also used (Borie et al, 1988) when the fields are expanded into TE_{mp} modes, p=1,2, ..., as would be strictly correct for the field profile in a complex cavity (a resonator containing a step, as discussed in Sect. 7). There it has been shown that the electron motion is determined mainly by the TE mode close to cutoff, thus supporting the assumption made by Fliflet et al (1988) in their self–consistent code for complex cavities.

To derive the adiabatic equation, one assumes the guiding center to be fixed and neglects the RF magnetic field, the effect of which is probably small for TE modes near cutoff, as is the case in a gyrotron oscillator (the approximation will be very poor for a device like a cyclotron autoresonance maser (CARM), which operates far from cutoff. Also, Salop and Caplan (1986) indicate that the RF magnetic field can have an important effect on the electron motion in the prebunching cavities of a gyroklystron).

The equation of motion for the transverse motion of the electron becomes, in complex phasor form, Fliflet et al, 1982)

$$i\dot{u}_t - (\dot{\Psi} - \Omega_0/\gamma)\, u_t = (a_r + i a_\theta)\, e^{i(\theta-\Psi)} + i\eta c u_z/2\gamma\, dB_0/dz\,(R_e\, e^{i(\theta_e-\Psi)} + r_L)$$
$$= -\eta\,(E_r + iE_\theta)\, e^{i\theta}\, e^{-i\Psi} + i\eta c u_z/2\gamma\, dB_0/dz\,(R_e\, e^{i(\theta_e-\Psi)} + r_L) \qquad (17)$$

We now assume that the RF electric field is described to sufficient accuracy by a linear superposition of modes of the form (1). Substituting (1) and(14) into (17) gives

$$i\dot{u}_t - (\dot{\Psi} - \Omega_0/\gamma)\, u_t = i\eta c u_z/2\gamma\, dB_0/dz\, (R_e\, e^{i(\theta_e - \Psi)} + r_L)$$
$$-i\eta/2\; e^{-i\Psi} \sum_{mp} C_{mp} k_{mp}\; e^{i\omega_{mp} t}\, V_{max}\, \hat{f}_{mp}(z)\; J_{m-1}(k_{mp} r)\, e^{-i(m-1)\theta}$$

$$du_z/dt = -\eta c u_t/2\gamma\, (r_L + R_e \cos(\Psi - \theta_e))\, dB_0/dz$$

Application of Graf's addition theorem (Abramowitz and Stegun, 1970) gives, with the slowly varying part of the gyrophase Λ defined by $\Lambda = \omega_a t - \Psi$, and neglecting all contributions except those corresponding to stationary phases corresponding to $\omega_{mp} \simeq s\omega_a$ (ω_a is an averaging frequency, approximately equal to Ω),

$$\dot{u}_t + i(\omega_a - \dot{\Lambda} - \Omega_0/\gamma)\, u_t = +\, (\eta c u_z r_L/2\gamma)\, dB_0/dz$$
$$-\eta/2 \sum_{mp} C_{mp} k_{mp}\, V_{max}\, \hat{f}_{mp}(z)\, J_{s-1}(k_{mp} r_L)$$
$$\times\, e^{i(\omega_{mp} - s\omega_a)t + is(\Lambda + \theta_e)}\, J_{m-s}(k_{mp} R_e)\, e^{-im\theta_e}$$

$$du_z/dt = -(\eta c u_t/2\gamma)\, r_L\, dB_0/dz \qquad (18)$$

In the fixed guiding center approximation, the initial azimuth θ_e (see figure 6) is approximately constant. For counter-rotating modes, $J_{m-s}(k_{mp}R_e)\, e^{-im\theta_e}$ should be replaced by $(-1)^s J_{m+s}(k_{mp}R_e) e^{im\theta_e}$. To compute the efficiency, one must average over both θ_e and initial gyrophase Λ_0.

For small values of the Larmor radius, one may take
$J_{s-1}(k_{mp} r_L) \simeq (k_{mp} c u_t/2\Omega_0)^{s-1}/(s-1)!$.
Assuming that $k_{mp} c/\Omega_0 \simeq 1$, this approximation is valid if $(u_t/2)^2 < 0.1$, or $\gamma\beta_\perp < 0.6$. For $\beta_{\perp 0} \simeq 0.4$, this means $\gamma_0 < 1.5$, or $U_{beam} < 250$ kV. Thus, the approximation is not valid for high voltage gyrotrons or CARM's. Assuming that the approximation is valid, and defining $P = iu_t e^{-i(\Lambda + \theta_e)}$, we have

$$dP/dt + i(\omega_a - \Omega_0/\gamma)\, P = (i\eta c u_z/2\gamma)\, dB_0/dz\, P/\Omega_0$$
$$-i\eta/2 \sum_{mp} C_{mp} k_{mp}\, V_{max}\, \hat{f}_{mp}(z)/(s-1)!\; J_{m-s}(k_{mp} R_e)\, e^{-im\theta_e}$$
$$\times \exp[(\omega_{mp} - s\omega_a)t])\, (ck_{mp}/2\Omega_0\, P^*)^{s-1}$$

with $\gamma = (1+u_z^2 + |P|^2)^{1/2}$. We now change variables from t to

$$z = \int_{t_0}^{t} cu_z/\gamma \, dt$$

For a single mode calculation, it suffices to average over the initial phase

$$\Lambda_0 + (1-m/s)\theta_e$$

and take $\omega_a = \omega_{mp}/s$. The average over θ_e then becomes trivial and one may ignore the explicit dependence on it. The result is

$$dP/dz + i\omega/cu_z \, (\gamma - \Omega_0/\omega) \, P = + i\eta/2 \, dB_0/dz \;\; P/\Omega_0$$
$$+ i\eta/2 \;\; \gamma/u_{z0} \, C_{mp} k_{mp} \, V_{max} \, (\hat{f}_{mp}(z)/(s-1)!) \, J_{m-s}(k_{mp}R_e) \, (ck_{mp}/2\Omega_0 \, P^*)^{s-1}$$

$$du_z/dz = - \eta cu_t r_L/u_z \;\; dB_0/dz \qquad (19)$$

For counter–rotating modes the factor $J_{m-s}(k_{mp}R_e)$ is replaced by $(-1)^s \, J_{m+s}(k_{mp}R_e)$. In the following, this factor will usually be denoted by G_{mp}. In much of the literature, the terms explicitly involving the magnetic field taper are neglected. In fact, it has been shown that for most cases of interest, the contribution to the efficiency is small (Gantenbein and Borie, 1990) and that the dominant contribution to the effect of magnetic field tapering is in the fact that the detuning depends on z. When these terms are neglected, the adiabatic equation of motion becomes a single complex differential equation:

$$u_z \simeq \text{constant},$$
$$dP/dz + i\omega \, /c\beta_{z0} \, (\gamma/\gamma_0 - \Omega_0/ \, \omega\gamma_0) \, P =$$
$$= i\eta/2 \;\; \gamma/u_{z0} \, C_{mp} G_{mp} k_{mp} \, \hat{f}_{mp}(z) \, (V_{max}/(s-1)!) \, (ck_{mp}/2\Omega_0 \, P^*)^{s-1} \, . \qquad (20)$$

The effect of space charge on the beam–field interaction has been neglected in the above. For most cases of interest, this is justified. Modifications to include this effect have been given by Bratman and Petelin (1975), and by Borie (1989). Borie used the distributed beam model of Kleva et al (1988), who calculated the effects of space charge on the operation of a quasi–optical gyrotron. The electromagnetic radiation in a gyrotron is generated by the azimuthal bunching of electrons in their gyro–orbits. This bunching is also a source of electrostatic fields, which then affect the electron motion.

The effects of space charge are added by considering the electrostatic potential produced in the distributed beam model (see Eq. (21) of Kleva et al 1988)

$$<q\phi/m> = -2q^2/4\pi\epsilon_0 m \int d^3u' f \int dt_0 \Omega_0/2\pi\gamma (\pi\Delta^2/2)$$

$$= -e^2/4\epsilon_0 m \int d^3u' f [u_\perp^2 + u'^2_\perp - 2 u'u \cos(\varphi-\varphi')]/ \Omega_0^2$$

Here f is the distribution function of guiding centers. The gradient of ϕ gives the electrostatic field which contributes to the equation of motion. After considerable manipulation, one finds, with $n_0 = \int d^3u' f$ and assuming that $\varphi-\varphi' \simeq \Psi-\Psi'$,$\Omega/\Omega_0 \simeq 1$

$$(a_x)_{SC} \simeq -\partial<q\phi/m>/\partial x$$

$$= e^2/4\epsilon_0 m [\Omega \cos\Psi \, \partial<q\phi/m>/\partial u_\perp - \Omega/u_\perp \, \partial<q\phi/m>/\partial \varphi]$$

$$= e^2/2\epsilon_0 m\Omega_0 [\cos\Psi \{u_\perp n_0 - \int d^3u' f u'_\perp \cos(\varphi-\varphi')\} - \sin\Psi \int d^3u' f u'_\perp \sin(\varphi-\varphi')]$$

$$= e^2/2\epsilon_0 m\Omega_0 [u_y n_0 - \int d^3u' f u'_\perp \cos \Psi']$$

Similarly

$$(a_y)_{SC} \simeq -e^2/2\epsilon_0 m\Omega_0 [u_x n_0 - \int d^3u' f u'_\perp \sin \Psi']$$

Hence the space charge contributions to the right hand side of (20) are

$$i\omega_p^2/2\Omega_0 \; [u_\perp - 1/n_0 \int d^3u' f u'_\perp (\cos(\Psi- \Psi') - i \sin(\Psi-\Psi'))]$$

where ω_p is the plasma frequency:

$$\omega_p^2 = e^2 n_0/\epsilon_0 m = 2\pi I_0/8500 A \Omega_0 c/4\pi R_e \beta_\perp \beta_z$$

(for an annular beam). The extra contributions to the right hand side of (20) are then (we ignore the dependence on θ_e, as is appropriate for a single mode calculation)

$$i\omega_p^2/2\Omega_0 \; [P + i/n_0 \int d^3u' f u'_\perp \exp(i(\Psi'-\omega t)] = i\omega_p^2/2\Omega_0 [P - 1/n_0 \int d^3u' f P'].$$

We now replace $1/n_0 \int d^3u' f P'$ by $N^{-1} \Sigma P_i = <P>$, where the average is over initial gyrophases, as before. The equation of motion then becomes

$$d P/dz + i\omega /c\beta_{z0} (\gamma/\gamma_0 - \Omega_0/ \omega\gamma_0) P =$$

$$= \eta/2 \; \gamma/u_{z0} C_{mp} G_{mp} k_{mp} \hat{f}_{mp}(z) V_{max} + i\omega_p^2/2\Omega_0 \; \gamma/cu_{z0} [<P> - P]$$

This form is computationally much easier to work with than the formulas given by Bratman and Petelin (1975), although the latter use a more realistic model for the beam. A similar term was found by Latham (1990) for gyroklystron amplifiers. Space charge results in some efficiency enhancement at very high power levels and a moderate reduction in efficiency at lower power levels when ω_p^2/Ω_0^2 is larger than about 0.005. This is equivalent to the

criterion given by Bratman et al (1981a), namely $(4/\pi\beta_\perp^2)\ \omega_p^2/\Omega_0^2 << 1$. Now

$$\omega_p^2/\Omega_0^2 = 2\pi I_0/8500\ A\ c/4\pi R_e\beta_\perp\beta_z\Omega_0 \simeq 9.4\times10^{-6}\ A^{-1}\ I_0\lambda/R_e\beta_\perp\beta_z$$

For the experiments at KfK in the TE_{03} mode, with λ=2.1 mm, R_e=1.82 mm, $\beta_\perp\simeq$0.4 and $\beta_z\simeq$0.26, this was about $10^{-4}\ A^{-1}\ I_0$, with I_0 < 15 A. The effect of space charge on the beam–field interaction was negligible (also in self–consistent calculations). For a more powerful gyrotron, the current increases, but a more highly overmoded gyrotron with a smaller value of λ/R_e is used, and the effect of space charge on the beam–field interaction in the resonator is probably no larger. The effect of space charge on beam quality (voltage depression) is probably more important from a practical viewpoint. The voltage depression has been discussed in detail by Drobot and Kim(1981) and by Ganguly and Chu (1984). The effective reduction in γ_0 will affect the detuning, and the effective value of α. This can be compensated by increasing the beam voltage, but at the price of a reduction in efficiency (Borie and Gantenbein, 1990). Beam instabilities may also play a role.

The electronic, or interaction efficiency η is calculated from the electron energy loss as follows. We observe that, since $\gamma = (1+u_z^2 + |P|^2)^{1/2}$,

$$d\eta/dz = 1/(1-\gamma_0)\ d<\gamma>/dz \quad \text{and} \quad \gamma\, d\gamma/dz = 1/2\ d|P|^2/dz\ .$$

Thus, the electronic efficiency is given by

$$\eta_{el} = (\gamma_0 - <\gamma(z_{out})>)/(\gamma_0 - 1)\ . \tag{21a}$$

The average < > is to be taken over initial gyrophase Λ_0 (in single mode approximation, averageing over θ_e is trivial). The electronic efficiency is also given by an integral over the beam–field interaction:

$$\eta_{el} = e/2m_ec^2\ C_{mp}G_{mp}k_{mp}\ V_{max(mp)}\ Im\left[\int_{z_{in}}^{z_{out}} P(z)\ \hat{f}^*_{mp}(z)\ dz\right]/[u_{z0}(\gamma_0 - 1)] \tag{21b}$$

Numerical checks show that the efficiency calculated with (21a) and (21b) is the same to within a fraction of a per cent, for the same parameters.

In the cold cavity approximation for the fields, the efficiency is a function of the field amplitude, or, equivalently, of the output power. For a steady state, $P = \eta(P)\ UI$. The steady state is stable if $dI/dP > 0$ and unstable if $dI/dP < 0$ (in this case, a self–consistent solution will not exist). The starting current I_{st} is the minimum current for which $dP/dt = \omega/Q\ (\eta(P)\ UI - P) > 0$ in the limit $P\to0$:

$$1/I_{st} = U\, d\eta/dP|_{P\to 0} \cdot \qquad (22)$$

Here it is assumed that $d\eta/dP|_{P\to 0} > 0$. Otherwise, oscillation will not start at the operating point under consideration. As an example, we show in Fig. 3.2 the beam current and efficiency as a function of output power. The numerical example is for a 150 GHz gyrotron considered for the KfK experiment (see Borie et al 1986), but shows several features which were pointed out earlier by Chu et al (1980). The resonator is for a $TE_{0,3}$ mode with R_0=3.24 mm, L_1= 10 mm, θ_1= 0.25°, θ_2= 0°, L_2= 10 mm, θ_3= 3°, L_3= 15 mm, F= 150.02 GHz, Q=1195. Note that the starting current is slightly larger than the minimum current for the beam voltage, magnetic field and value of α used here. These parameters were selected for good efficiency at 200 kW. For the case under consideration, the starting current is only slightly lower than the current corresponding to $\eta \simeq 50\%$ at 200kW. Oscillation can start at currents slightly above the starting current, but the system

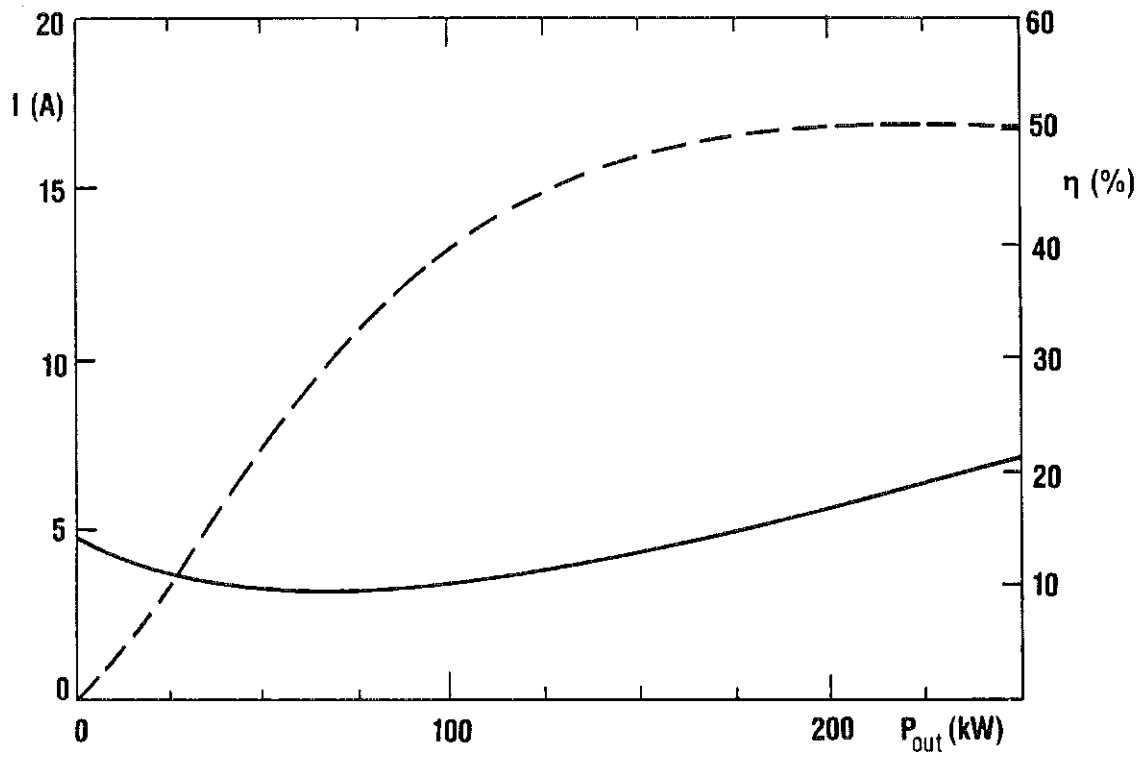

FIG. 3.2: Beam current (solid curve) and efficiency (dashed curve) as a function of output power for the TE031 mode in a resonator with the geometry R_0=3.24 mm, L_1= 10 mm, θ_1= 0.25°, θ_2= 0°, L_2= 10 mm, θ_3= 3°, L_3= 15 mm, F= 150.02 GHz, Q=1195. Here U_b=70 kV, α = 1.5, B=5.82 T, $\Delta B/B$ = 2% and the beam is placed at the second radial maximum of the RF field.

will jump to a stable steady state having output power over 100 kW. The region of parameter space in which the starting current exceeds the current is called the hard excitation region. In some cases, the parameters corresponding to optimum efficiency lie in the hard excitation region, making access difficult. In general, startup is easier, in the sense that the starting current is smaller compared with the current at maximum efficiency for the parameters under consideration, and the high efficiency region is more easily accessed, if the magnetic field is increased slightly. If this can be done without an overly large decrease in efficiency, it is probably desirable to do this. In addition, stability with respect to perturbations by a lower frequency parasitic mode will be improved.

The starting current can, of course, also be calculated in a linearized single mode theory. This has been done in a number of ways by Petelin and Yulpatov (1974) (see also Petelin 1981), Kreischer and Temkin (1983), Sprangle and Drobot (1977), Chu (1978), Nusinovich (1988), Borie and Jödicke (1988). We do not give the derivation again here. The result is:

$$-1/I_{st} = QZ_0\,(\pi/\lambda \int |\hat{f}(z)|^2 dz)^{-1}\, e/8\gamma_0 m_e c^2\, (k_{mp}C_{mp}G_{mp}/\beta_{z0})^2 \times[1 + \tfrac{1}{2}\,\omega\beta_{\perp 0}^2/v_{z0}\;\partial/\partial\Delta_1] \int_0^L \hat{f}(z)\, e^{i\Delta_1 z} dz|^2 \qquad (23)$$

Here $\Delta_1(z) = \omega/v_{z0}\,(1 - \Omega_0(z)/\omega\gamma_0)$. The factor

$$\pi(C_{mp}G_{mp})^2 = J^2_{m\pm1}(x_{mp}R_e/R_0)/[(x^2_{mp}-m^2)J^2_m(x_{mp})]$$

is the usual beam–field coupling coefficient. The single mode starting currents calculated with the linear theory give the same numerical results as those calculated by extrapolating the nonlinear theory to low power levels (a few kW). This provides a good check on the approximation (Borie and Jödicke, 1988). We shall show later, that this is not always the case when dealing with mode competition.

If the RF field is a linear superposition of corotating and counterrotating components (this can occur, for example, when the beam is not exactly centered on the resonator axis or is not perfectly homogeneous and m≠0), then the RF field has the form

$$E_\theta = C_{mp}k_{mp}\, J'_m(k_{mp}r)\, e^{i\omega t}\, \hat{f}_{mp}(z)\, (V_+\, e^{im\theta} + V_-\, e^{-im\theta})$$

$$E_r = -i\, C_{mp}k_{mp}\, (m/k_{mp}r)\, J_m(k_{mp}r)\, e^{i\omega t}\, \hat{f}_{mp}(z)\, (V_+\, e^{im\theta} - V_-\, e^{-im\theta})$$

with $V_+ = V_{max}\sin\Theta\, e^{+i\chi}$ and $V_- = V_{max}\cos\Theta\, e^{-i\chi}$.

Θ is an arbitrary parameter, analogous to the mixing angle used commonly in particle physics (see Halzen and Martin 1984), and χ defines the relative phase of the two components. It is well–known that this linear combination is the most general one possible. This choice preserves the normalization of the basis states, as is shown in any text on linear algebra. Also, we follow Feynman (1965) in distributing the relative phase symmetrically over the two components. Other conventions are possible, but the symmetric one is, in this author's opinion, the most useful. For standing waves, $\Theta = \pi/4$. If the cavity is slotted, this choice gives the appropriate normal modes, as was pointed out by Petelin (1981). For a slightly elliptical or displaced beam this is unlikely to be the correct choice. The mixing angle should be a continuous function of beam eccentricity. In this case, the factor G_{mp} in (20) should be replaced by

$$[\cos\Theta\, e^{-i(\chi+m\theta_e)}\, J_{m-s}(k_{mp}R_e) + (-1)^s \sin\Theta\, e^{i(\chi+m\theta_e)}\, J_{m+s}(k_{mp}R_e)] \qquad (24)$$

The average over θ_e is then equivalent to an average over $\chi/m+\theta_e$ and the relative phase disappears trivially. For practical calculations, it is preferable to remain with a linear superposition of two modes, rather than to try to combine (24) into amplitude and phase. This formulation retains more explicitly the basic linearity of Maxwell's equations and is computationally less intensive. In the linearized theory, after averaging ove θ_e, one obtains the expression (23) for the starting current, except that G_{mp}^2 is replaced by

$$\cos^2\Theta\, J_{m-s}^2(k_{mp}R_e) + \sin^2\Theta\, J_{m+s}^2(k_{mp}R_e)$$

This is an obvious generalization of the formula for standing waves given by the Gorky group (Petelin, 1981).

IV. SELF–CONSISTENT CALCULATIONS

In a self–consistent calculation, the equations of motion for the electrons are solved simultaneously with the field equations, taking the effect of the beam on the cavity field profile and quality factor, as well as frequency pulling, into account. These effects are important for gyrotron operation. A self–consistent model for the gyrotron, very similar to what will be presented here, was first given by Bratman (1973). The model derived here is basically that due to Fliflet et al (1982), although the algorithms used to solve the equations numerically are probably different. A similar, equivalent model has been given by Charbit et al (1981). Here, we give the equations for arbitrary harmonics, and discuss some aspects

of the numerical methods which have been used successfully in Karlsruhe. We assume that the RF electric field is described to sufficient accuracy by a single TE_{mp} mode, with field profile described to sufficient accuracy by the Vlasov (1969) equation (13). The equation of motion is then as given above (20). Note that this assumption neglects distortion of the transverse structure of the RF field by the beam. It remains to determine the current term J_{mp}. The current due to electrons in an annular beam is assumed to be given by

$$\vec{J} = \Sigma q_i \vec{v}_i \ \delta(r_i - R_e - r_L \, e^{i(\Omega \tau_i + \phi_i - \phi_{0i})})/2\pi R_e . \qquad (25)$$

q_i is the charge of the i th electron and $\vec{v}_i$ is its velocity. The total current is given by

$$-I_0 = \int J_z \, dA .$$

Inserting (25) into (9) gives

$$J_{mp} = \mu_0/2\pi R_e \ \partial/\partial t \int \Sigma q_i \ \delta(r_i - R_e - r_L \, e^{i(\Omega \tau_i + \phi_i - \phi_{0i})}) \ \vec{v}_{ti} \cdot \vec{e}^{\,*}_{mp} \, dA$$

Following Fliflet et al (1982) we have

$$1/2\pi R_e \int \delta(r - R_e - r_L \, e^{i(\Omega \tau + \phi - \phi_0)}) \ \vec{v}_t \cdot \vec{e}^{\,*}_{mq} \, dA$$
$$= \mp C_{mq} k_{mq} J_{m\pm1}(k_{mq} r) \, e^{-i(1\pm m)\theta} \ v_t \, e^{i(\Omega \tau + \phi - \phi_0)} .$$

Using Graf's theorem, and assuming the gyration radius to be small gives for corotating components (corresponding to the lower sign)

$$[d^2/dz^2 + \omega_{mq}^2/c^2 - k_{mq}^2(z)] \, V_{mq} \ e^{i\omega_{mq} t}$$
$$= -\mu_0 I_0 \, C_{mq} k_{mq} \, \Sigma \, J_{m-s}(k_{mq} R_e)/[2^{s-1}(s-1)!]$$
$$\times \partial/\partial t \ \Sigma \, u_{ti}/u_{zi} \, e^{is(\Omega \tau_i + \phi_i - \phi_{0i})} \, (ck_{mq} u_{ti}/\Omega_0)^{s-1} \, e^{i(m-s)\theta_e}$$

Introducing $P = iu_t \, e^{-i\Lambda}$ and selecting a single harmonic s gives ($\Lambda = \omega_a t - \Omega\tau - \phi$) with ω_a as defined in the previous section.

$$[d^2/dz^2 + \omega_{mq}^2/c^2 - k_{mq}^2(z)] \, V_{mq} \, e^{i\omega_{mq} t}$$
$$= -Z_0 I_0 \, C_{mq} k_{mq} \, e^{im\theta_e} \ J_{m-s}(k_{mq} R_e)/[2^{s-1}(s-1)!]$$
$$\times \Sigma \, (is\omega_a \, P_i + \partial P_i/\partial t)/cu_{zi} \ (ck_{mq} P_i/\Omega_0)^{s-1} \, e^{is(\omega_a t_i - \theta_e)} \qquad (26)$$

For counterrotating components, the factor $J_{m-s}(k_{mq}R_e)\, e^{im\theta_e}$ should be replaced by $(-1)^s J_{m+s}(k_{mq}R_e)\, e^{-im\theta_e}$. $Z_0 = \mu_0 c \simeq 377\ \Omega$.

Here t_i is the time at which the i'th electron passes $z = \int \gamma_0 v_{z0}/\gamma\, dt$. We wish to use the trajectories of a representative group of electrons as they move through the resonator. Since the behavior of the system is periodic, for any electron passing through a plane $z=z_0$ outside any cycle of interest, there is another one within some cycle an integral number of cycles sooner or later which will contribute the same amount to the sum in (26). Hence the summation can be taken over all the electrons passing an initial plane within one cycle. In addition, the sum must extend over initial electron azimuth θ_e. For a single mode calculation it suffices to average over the initial phase $\Lambda_0 + (m/s-1)\theta_e$. This gives

$$d^2V_{mq}/dz^2 + [\,\omega_{mq}^2/c^2 - k_{mq}^2(z)]\, V_{mq} = -Z_0 I_0\, C_{mq} k_{mq}\, G_{mq}/(s-1)!\, (\omega_{mq}/cu_{z0})\, (-ick_{mq}/2\Omega_0)^{s-1} < P^s > \qquad (27)$$

For completeness, we repeat the equation of motion:

$$dP/dz + i\omega/c\beta_{z0}\, (\gamma/s\gamma_0 - \Omega_0/\omega\gamma_0)\, P = i\, G_{mp} C_{mp} k_{mp}(z)\, (\gamma/\gamma_o\beta_{z0})\, V_{mp}(z)/1022kV\, (ck_{mp}P^*/2\Omega_0)^{s-1} \qquad (20)$$

Recall that $G_{mp} = J_{m-s}(k_{mp}R_e)$ for corotating modes and $(-1)^s J_{m+s}(k_{mq}R_e)$ for counterrotating modes.

For numerical calculations, the boundary condition at z_{in} is used to determine the starting value of dV/dz for the integration of (27) and the boundary condition at z_{out} is reformulated in the form

$$|R| = |(dV/dz + ik_z V)/(dV/dz - ik_z V)| = \text{minimum}$$

When a source is present, the eigenfrequency of a steady state solution is real, in contrast to the cold cavity case, in which the eigenfrequency has a positive imaginary part to account for damping due to radiation out of the cavity. The normalization of the field profile is now determined by the source term and this is reflected in the fact that the coupled equations plus boundary conditions cannot be satisfied for arbitrary values of the initial value $V(z_{in})$. For this reason the most efficient method of solution is to solve the coupled equations (20) and (27) simultaneously, and vary the values of ω and $|V(z_{in})|$ until $|R|$ is

minimized. Note that the derivative of V at the input is given by the initial condition $V'(z_{in}) = \kappa_{mp} V(z_{in})$, where

$$\kappa_{mp} = [k^2_{mp}(z_{in}) - \omega^2_{mp}/c^2]^{1/2} .$$

Some authors specify $V'(z_{in})$. When $V(z_{in})$ is then specified by the initial condition, this is completely equivalent. If, as is almost always the case, $|V(z_{in})| << V_{max}$, there is no numerical difference compared with setting $|V(z_{in})| \simeq 0$.

For the numerical solution of the coupled equations (20) and (27) it turned out to be computationally very advantageous to use a simple predictor–corrector method for the equation of motion (20) and the leapfrog algorithm (Hockney and Eastwood 1981) for the field equation. The reason for this is that the derivatives dV/dz are evaluated at points midway between the points at which P and f are evaluated (see Fig. 4.1), with the result that only preceding values of <P> are used in the computation of the subsequent value of dV/dz. Since one may wish to average over 30 initial gyrophases, the advantage of only having to evaluate <P> once at each step of the integration is obvious.

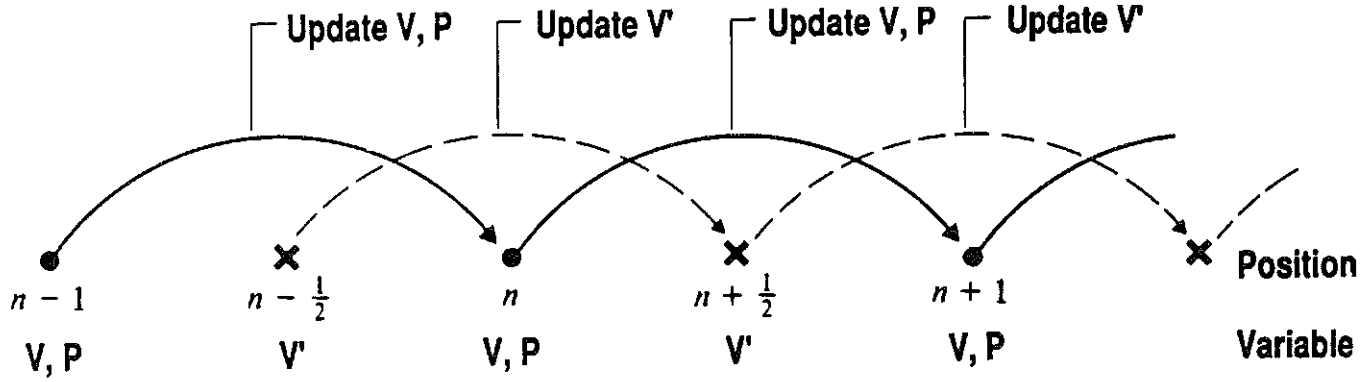

FIG 4.1. The field equation is integrated using the leapfrog scheme. V at position n–1 is updated using V' at position n–1/2; then the set of P's (one for each initial gyrophase) at position n–1 is updated using V at position n–1 and at position n. Then V' at position n–1/2 is updated using V and <P> at position n, and so forth.

The output power is determined by (11):

$$P_{out} = \mathrm{Re}\,(1/2\,\mu\omega)\,k^{*}_{zmp}\,|V_{mp}(z_{out})|^2\,.$$

If the solution is really self consistent, this will also be equal to

$$P_{out} = \eta_{el}\,U_0\,I_0.$$

This can be used the check the quality of the solution. The quality factor can then be found from (15).

$$Q\,P_{out} = \omega\,W = \omega\,\epsilon_0/2 \int_{z_{in}}^{z_{out}} |V_{mp}(z)|^2\,dz.$$

In general, the quality factor determined in a self–consistent calculation is somewhat larger than the cold cavity Q. This effect is partly numerical. At the cavity output, the function V(z) has the form

$$V(z) \simeq e^{-ik_z z}$$

with $k_z^2 = \omega^2/c^2 - k_{mp}^2(z_{out})$. If ω is complex, then k_z is also. The sign of the imaginary parts of k_z is the same as that of ω. Thus, there is a small exponential increase in the function $V_{cc} \sim \exp(\omega z/2Qc)$ for the cold cavity field profile which is absent in the self–consistent field profile, for which ω is real. At sufficiently large values of current, another effect also tends to increase the quality factor. This has been described by Bratman (1973) as "overbunching". The electronic efficiency reaches a maximum somewhere before the end of the resonator, and the field strength becomes so large that the electrons gain energy from the RF field. The efficiency drops again, resulting in more energy stored in the field and less output power for a given current. This is one reason why maximum output power is achieved for other parameters than maximum efficiency. If overbunching becomes too severe, the maximum local wall losses will be too large. For this reason, the gyrotron should be operated at parameters for which this does not occur. We illustrate these points with two examples.

Fig. 4.2 shows field profiles for the resonator designed to operate in the TE10,4 mode which was used as an example in the section on waveguide cavities. It has R_0=8.11 mm, θ_1=5°, L_1=10 mm, θ_2=0°, L_2=11 mm, θ_3=3°, L_3=12 mm. In the cold cavity approximation the frequency is 140.13 GHz, and Q=590. For an output power of 762 kW, U=80 kV, α=1.8 and B=5.52 T, the electronic efficiency is 46.8%, corresponding beam current 20.3 A, and maximum wall loading (for ideal hot copper) 3 kW/cm^2. The field profile $|\hat{f}(z)|$ is the solid curve. The result of a self–consistent calculation for the same beam voltage, α and magnetic field, and I=20 A is shown by the dashed curve. Now

F=140.21 GHz (frequency pulling), Q=701, P=762 kW, η_{el}=47.8%, maximum wall loading 4 kW/cm^2. Most of the increase in Q is due to the numerical effect discussed above. The power and efficiency do not differ much from the cold cavity calculation. The dash–dot curve shows the effect of overbunching. Here the current is 35 A, and all other parameters are as before. Now F=140.30 GHz, Q=969, P=767 kW, η_{el}=27.3%, maximum wall loading 6 kW/cm^2. An examination of η_{el} as a function of z in this case would show that the electrons give up nearly half their energy midway through the cavity and are then reaccelerated, accounting for the low output efficiency. Since the field energy in the resonator is high, and the output power low, the quality factor must increase, and with it the wall loading for a given output power.

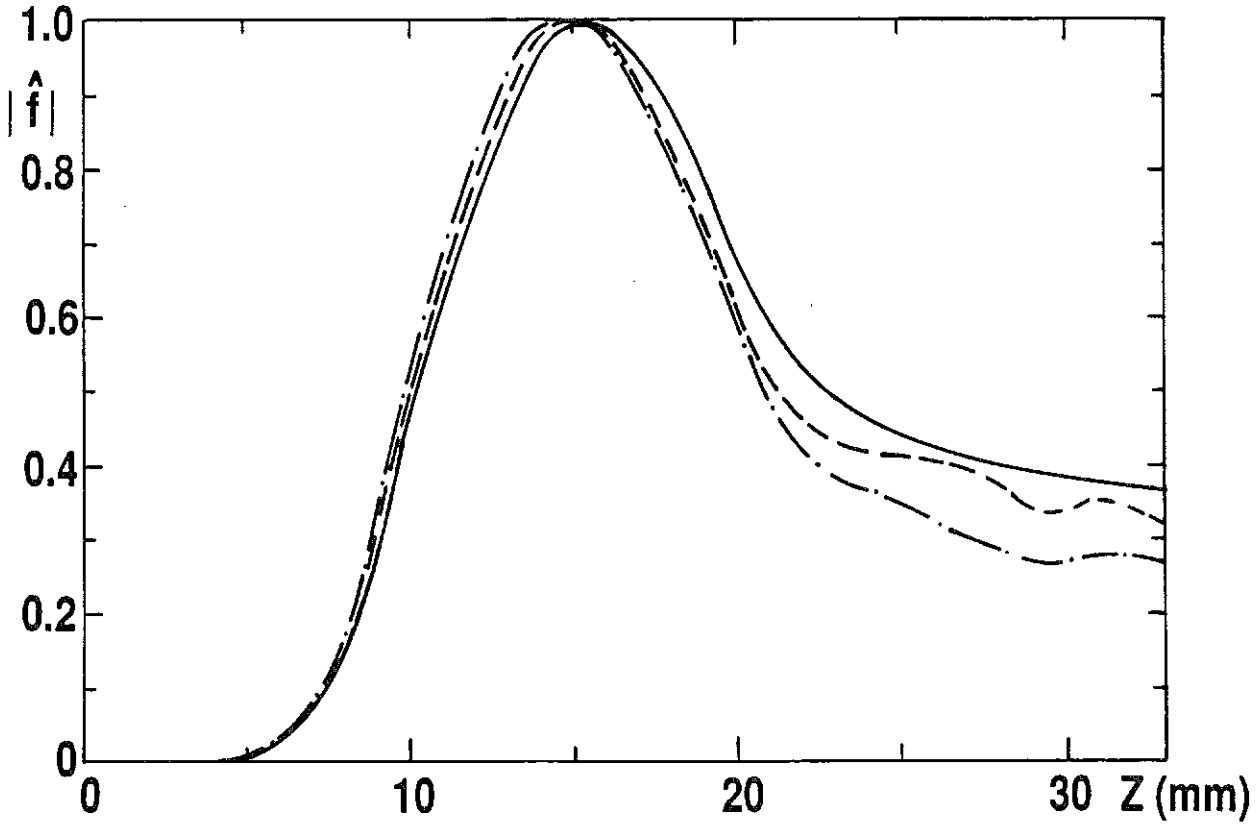

FIG. 4.2 normalized field profiles for the TE10,4 mode in a resonator with R_0=8.11 mm, θ_1=5°, L_1=10 mm, θ_2=0°, L_2=11 mm, θ_3=3°, L_3=12 mm. Solid curve: cold cavity. F=140.13 GHz, Q=590. dashed curve: self–consistent for I=20 A. F=140.21 GHz, Q=701. dash–dot curve: self–consistent for I=35 A. F=140.30 GHz, Q=969.

Fig. 4.3 shows contour plots of the efficiency of the TE10,4 mode as a function of magnetic field and current for the same resonator as in the previous figure. The calculations were performed for beam voltage 80 kV and α=1.8. The results are plotted in terms of the dimensionless parameters $I=\pi I_0/8517$ A $\beta_{z0}/\gamma_0 (C_{mp}G_{mp})^2$ and $\delta=1-\omega_{c0}/ck_{mp}\gamma_0$. The values correspond to $0<I_0<30$ A and 4.67 T $< B/\gamma_0 <$ 4.95 T. Fig. 4.3a shows the result of a cold cavity calculation. The solid curve shows the minimum current and the dash–dot curve the starting current. Maximum efficiency is expected in the hard excitation region. Fig. 10b shows the corresponding contours calculated self–consistently. The minimum current is increased somewhat for all values of δ. The regions of highest efficiency are similar to those of the cold cavity case (this is typical), but the efficiency drops rapidly at higher currents due to overbunching. A good operating point should be somewhat above the minimum current, but not too far into the region of severe overbunching. For the example considered here, this should be achievable at an output power of about 1/2 MW, with an electronic efficiency somewhat over 40% at a current of about 18 A, and wall loading 2–3 kW/cm^2. Maximum efficiency occurs at over a megawatt, with intolerably high wall loading (for CW operation). Operation at maximum efficiency for power levels of 1/2 MW is possible, but only with a longer, higher Q resonator and a corresponding increase in wall loading. The cold cavity calculations can give a good first overview of the desired parameter region, but must be supplemented with self–consistent calculations.

The starting current can also be calculated self–consistently. The formalism for the linearized theory has been given by Bratman et al (1981). It is, however, no easier to solve the resulting integro–differential equation than it is to use the nonlinear formalism, with the value of V_{mp} at the input fixed at the cold cavity value corresponding to a small value of P_{out} (eg 1 kW) and varying the frequency and current until a solution obeying the radiation boundary condition at the output is found. The starting current curves calculated in a self–consistent theory differ somewhat from those calculated with a fixed field profile. Here we show results calculated with both methods for the TE_{03} mode and a resonator having $\theta_2=0^\circ$ and L_2=10 mm. This is due to the fact that the beam excites a backward wave as well as a forward wave, as pointed out by Bratman et al (1981a) and Fliflet et al (1982). At higher magnetic fields, the backward wave becomes more important. At the highest magnetic fields, the backward wave becomes so important that the self–consistent solution becomes ill–defined. Frequency pulling is also important, and is never described well by linear theory (Kreischer et al 1984b) or by perturbation theory (Borie, 1986). Fig. 4.4 shows the starting current for several values of magnetic field taper for three cases: a) adiabatic

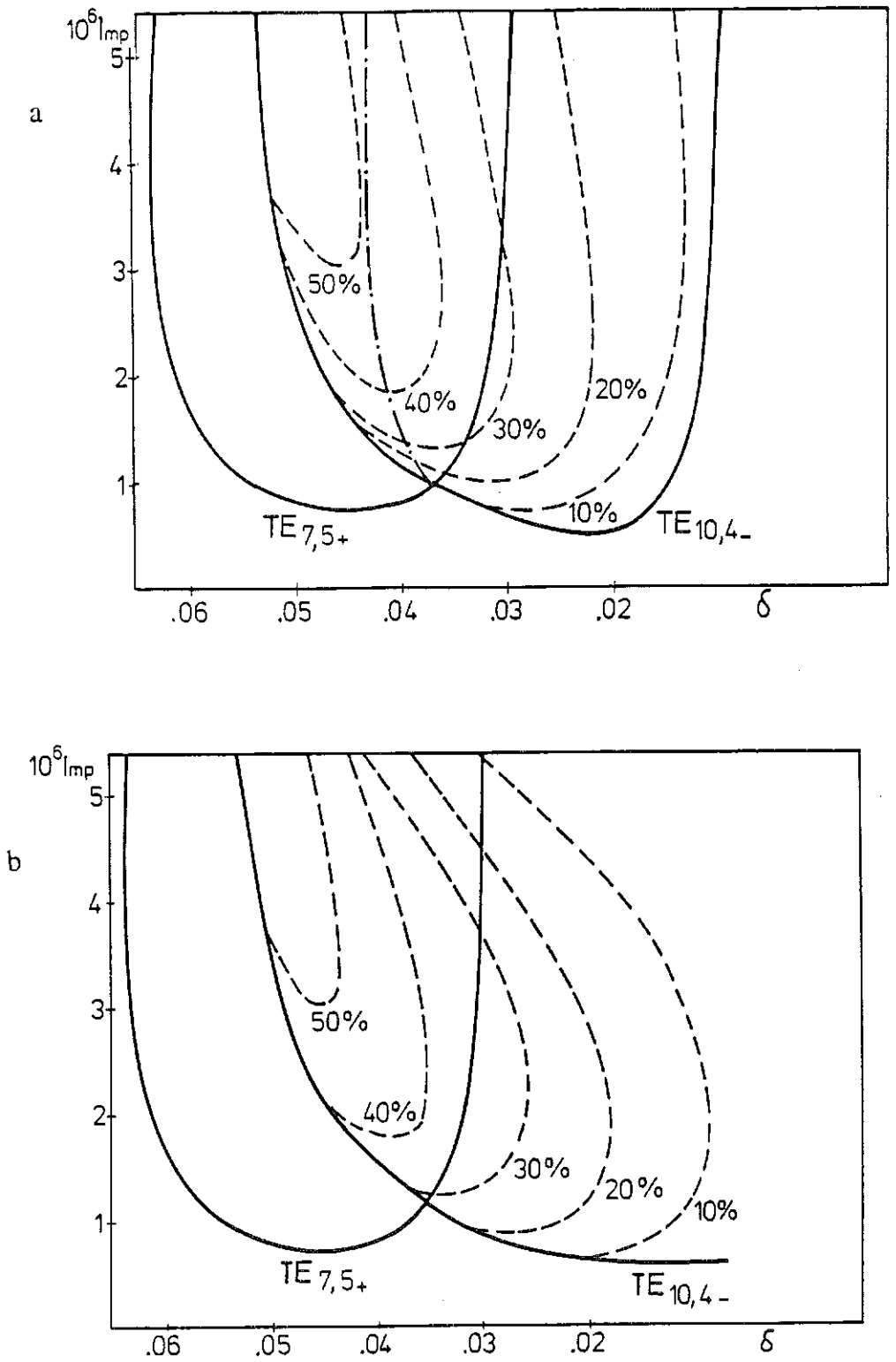

Fig. 4.3 Contours of constant efficiency in the I – δ plane, calculated for the same resonator as in Fig. 4.2, with α=1.8 and accelerating voltage 80 kV. (a) cold cavity and (b) self–consistent. See text for definition of I and δ.

equation of motion, cold cavity field profile. b) exact equation of motion, cold cavity field profile. c) adiabatic equation of motion, self–consistent. The difference between the cold cavity calculations is very small. The self–consistent calculation shows significant differences. The curves in Fig. 4.4(a) can be obtained either from the linearized theory or from an extrapolation of the nonlinear theory to low output power. The results are identical, and do not agree with calculations based on a Gaussian field profile (Borie and Jödicke, 1988).

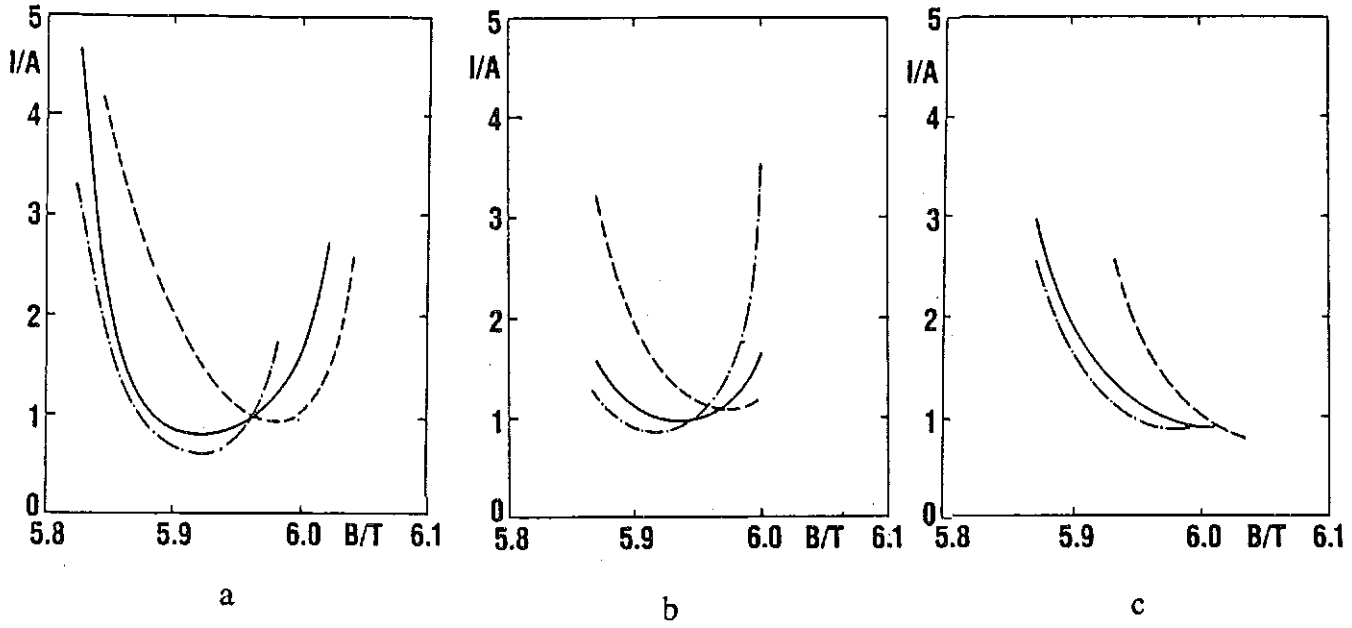

Fig. 4.4. Starting current of the TE03 mode as a function of magnetic field for several values of magnetic field tapering. The resonator is 10 mm long with a radius of 3.24 mm and frequency about 150 GHz. Beam voltage is 70 kV and α=1.5. Solid curves: $\Delta B/B = 0$. Dashed curves: $\Delta B/B = +5\%$. Dash–dot curves: $\Delta B/B = -2.5\%$. a) cold cavity approximation, with adiabatic equation of motion for the electrons. b) cold cavity approximation, exact equation of motion for the electrons. (c) self–consistent theory, adiabatic equation of motion.

V DIMENSIONLESS VARIABLES

A number of different sets of dimensionless variables have been proposed and used by various authors or groups of authors. These can be very helpful in analysing gyrotron behavior independent of inessential parameters. The choice depends partly on the application and/or approximations used, and partly on the taste of the user.

The Gorky group (see eg Nusinovich 1986, Danly and Temkin 1986) reduces their equations in terms of the variables

$$\mu = \pi L/\lambda\ (\beta_{\perp 0}^2/\beta_{z0}),\quad \zeta = \pi z/\lambda\ (\beta_{\perp 0}^2/\beta_{z0})$$

$$\Delta_G = 2/\beta_{\perp 0}^2\ (1 - s\Omega_0/\omega\gamma_0)$$

$$F_G = 2/\beta_{\perp 0}^2\ (eV_{max}/2m_ec^2)\ (C_{mp}G_{mp})/u_{t0}\ (s\beta_{\perp 0}/2)^{s-1}/s!$$

and, for self–consistent calculations

$$I_G = (2/\beta_{\perp 0}^2)^{4-s}\ (eZ_0I_0/2m_ec^2)\ \beta_{z0}\ (C_{mp}G_{mp})^2\ s\ [s/(s-1)!]^2\ .$$

Here L is the effective length of the field profile, usually taken to be the length of an equivalent Gaussian field profile of the form $\exp[-(2z/L-1)^2]$.

Other possible sets of dimensionless variables have the advantage that the integration variable is not so sensitive to the (poorly known) pitch angle α. For example, define

$$\delta = 1 - \Omega_0/(\omega\ \gamma_0),\quad \tilde{P} = P/u_{t0},\quad \tilde{z} = \omega\ z/v_{z0}\ .$$

Further let

$$F_{mp} = eV_{max}/2m_ec^2\ (C_{mp}G_{mp})/u_{t0}\ (ck_{mp}/\omega)\ \text{ and}$$

$$I_{mp} = eZ_0I_0/2m_ec^2\ \beta_{z0}\ (C_{mp}G_{mp})^2/\gamma_0\ (ck_{mp}/\omega)^2\ .$$

Note that these are related to the variables used by the Gorky group by

$$\zeta = \tilde{z}\ \beta_{\perp 0}^2/2\ ,\ F_{mp} = \beta_{\perp 0}^2/2\ (ck_{mp}/\omega)\ F_G\ ,\ I_{mp} = (\beta_{\perp 0}^2/2)^3\ (ck_{mp}/\omega)^2\ I_G/\gamma_0 \text{ and}$$

$\delta = \beta_{\perp 0}^2/2\ \Delta_G$ (for the first harmonic), and to those used by Antonsen et al (1989), who use

$$\delta_A = L\omega/2v_{z0}\ \delta\ =\ \text{transit angle (Bratman et al 1981a)}$$

$$\epsilon_A = eV_{max}/2m_ec^2\ (C_{mp}G_{mp})/u_{t0}\ L\omega/v_{z0} = \mu\ F_G = L\omega/v_{z0}\ F_{mp}\ (\omega/ck_{mp}).$$

The self–consistent system of equations given in the previous section can then be written in the form ($\hat{f}_{mp}$ is the field profile normalized to $|\hat{f}|_{max}=1$)

$$d\tilde{P}/d\tilde{z} + i\ (\gamma/\gamma_0 - 1 + \delta)\ \tilde{P} = i\ \gamma/\gamma_0\ F_{mp}\ \hat{f}_{mp}(z) \qquad (20')$$

and

$$[d^2/d\tilde{z}^2 + \beta_{z0}^2\ (\omega^2 - c^2k_{mp}^2(\tilde{z}))/\omega^2 + I_{mp}]\ F_{mp}\ \hat{f}_{mp} = -I_{mp}\ \Omega_0/\omega\ <\tilde{P}/\gamma> \qquad (27')$$

In this form, the equations are clearly quite general. The free parameters are $\delta_0 = 1 - \Omega_0/(ck_{mp}\gamma_0)$ and I_{mp}, as well as the resonator geometry. These determine ω (and thus δ, which depends on the frequency pulling) and $F_{mp}\hat{f}_{mp}$.

The system of equations used by the Gorky group (see, eg Bratman et al 1973), is easily obtained from these by setting $ck_{mp}/\omega \simeq 1$ (except in the field equation), $\gamma/\gamma_0 - 1 \simeq (\beta_\perp^2 - \beta_{\perp 0}^2)/2 \simeq \beta_{\perp 0}^2/2\,(|\tilde{P}|^2 - 1)$, $\gamma_0 \simeq 1$ elsewhere, and transforming variables from $\tilde{z}$ to ζ. These approximations are adequate for beam voltages less than about 100 kV, but may not be sufficiently accurate at higher voltages. Suitable dimensionless variables for relativistic gyrotrons and other cyclotron resonance masers have been introduced by the Gorky group, and the physics of such devices is discussed by Bratman et al, 1981b, Petelin, 1974 and Fliflet, 1986.

For cold cavity calculations, the variables μ, Δ_G and F_G provide a very compact description of the essential features of gyrotron behavior, within the limits of the approximations made. In a self–consistent calculation, both μ and Δ will be modified from the input values by frequency pulling and distortion of the field profile. As has been pointed out by Bratman et al (1975), the value of μ at which optimum efficiency occurs is reduced to 14.5 from the Gaussian cold cavity value of 17. Even then, overbunching can occur if the beam current parameter is too large. Also, by choosing an even shorter resonator (smaller value of μ), it is possible to raise the maximum output power with only a modest sacrifice in efficiency, since the quality factor is decreased, and with it the wall loading (Bykov and Goldenberg 1975). Antonsen and Levush (1989) point out that devices having a smaller value of μ have larger stable operating regimes. Such tradeoffs limit the value of the widely popular μ–F contour plots (which do not appear at all in the Gorky Collected Papers, 1981). They are of some use for a first orientation in parameter space, but must be supplemented by self–consistent calculations over a fairly large region of the parameter space of interest, considerations of wall loading, voltage depression (Drobot and Kim, 1981, Ganguly and Chu, 1983) and of mode competition. For fairly low order modes, at moderate frequencies ($x_{mp} < 10$), where such issues are not so important, this approximation is adequate; otherwise additional analysis is needed, and is generally carried out. In the case of mode competition, both frequencies are pulled, and both field profiles are distorted (but not the same way). The number of free parameters rapidly becomes as large as is the case for all other sets of variables. Aside from independence of the explicit mode, one gains little by using these variables. Other formulations of dimensionless variables also offer this advantage, and the choice of variables then becomes purely a matter of taste and convenience.

OTHER POSSIBILITIES

Particle in cell simulation codes, which have been described in Hockney and Eastwood (1981), Birdsall (1987), Dawson, (1983) are widely used in some plasma physics applications, but have not been used much to calculate RF behavior in gyrotron oscillators. One reason is probably the success of the theory presented here in describing the essential features of RF behavior in gyrotron oscillators. Caplan et al (1983) have used a PIC–type code to simulate the saturated behavior of a gyrotron amplifier. The transverse field structure was fixed and assumed to be the same as that of an empty waveguide mode. The variation of the RF field with z and t was solved self–consistently with relativistic particle trajectories. The beam was simulated by several thousand test particles. A matched RF absorbing region beyond the beam exit permitted the calculations to be performed in a closed region. Output power was calculated using Poynting's theorem. Such a code can model transient behavior and the effect of velocity spread well. The effect of an off–center beam would require variation in more dimensions that the two (z,t) considered here. The computational effort required may be more than is necessary to describe the nearly stationary states which characterize the operation of gyrotron oscillators having long pulses and moderate voltages and currents, but this method may be a very useful tool for describing the transient behavior in high voltage, short pulse gyrotrons. This point will be discussed further in connection with mode competition in the next section.

VI MODE COMPETITION

The theory of a multimode gyrotron was first investigated by Moiseev and Nusinovich (1974). This theory was further developed by Nusinovich (1981, 1986), and adapted and compared with experiment by Dialetis and Chu (1983), Kreischer et al (1984c) , Vomvoridis (1982), Borie and Jödicke (1987), Riyopoulos (1990), and by Levush and Antonsen (1990).

The starting point for a calculation of mode competition is the equation of motion for an electron in the field produced by a superposition of modes. This has been derived in the section on equation of motion. One must then consider the power transfer from the electrons to each individual mode and determine the possible equilibrium states.

Here, for consistency of notation, we present the theory in the form used by Borie and Jödicke (1987, 1991). The Gorky formalism is, as has been discussed before, completely equivalent, and many ideas presented here were originally discovered by the Russian authors. As usual, if $P = iu_t\, e^{-i\Lambda}$ describes the transverse component of the electron momentum , we have from equations (18), (19)

$$d P /dz + i\omega_a /c\beta_{z0} (\gamma/\gamma_0 - \Omega_0/ \omega_a\gamma_0) P =$$
$$= -i\gamma/cu_{z0} \sum_{mp} \tilde{F}_{mp}\, \hat{f}_{mp}(z) \exp[i\psi_{mp}] (ck_{mp}/\Omega_0\, P^*)^{s_{mp}-1} \qquad (28)$$

with $\gamma = (1+u_z^2 + |P|^2)^{1/2}$, $\psi_{mp} = (\omega_{mp}-s_{mp}\, \omega_a)t+(s_{mp}-m)\theta_e$, and

$$\tilde{F}_{mp}(z) = |e|V_{max}/2m_ec^2\, C_{mp}G_{mp}\, (ck_{mp}(z)) /[2^{s_{mp}-1}\, (s_{mp}-1)!]$$

Recall that $G_{mp} = J_{m-s_{mp}}(k_{mp}R_e)$ for corotating modes and $(-1)^{s_{mp}} J_{m+s_{mp}}(k_{mp}R_e)$ for counterrotating modes (for which the sign of m in the right hand side of (28) also changes). As discussed previously, θ_e is the initial azimuth of the electron in the hollow beam. In the fixed guiding center approximation, it is constant for each electron. In a single mode calculation the dependence on θ_e is included in the definition of Λ. When several modes having different azimuthal index are assumed to be present simultaneously, this cannot be done. ω_a is an averaging frequency, and was first introduced by Nusinovich (see, eg Nusinovich, 1981, 1986). Numerically, it is close to the cyclotron frequency. The final results can be shown to be independent of ω_a.

In the case of gyrotrons operating in a whispering gallery mode, two kinds of mode competition are possible (Nusinovich, 1981, 1986). The first, and for this discussion most important, is the ordinary competition between two modes with purely amplitude

interaction. The second kind of competition which can occur is the competition between modes due to phase–amplitude interaction. This would be competition between the operating $TE_{m,p}$ mode and the parasitic, nearly equidistant satellites: $TE_{m-1,p}$ and $TE_{m+1,p}$. Although this kind of mode competition is dominant in quasi–optical gyrotrons (Antonsen et al (1989), Riyopoulos, 1990)), it is in many cases less important in the case of circular gyrotron oscillators. The spacing of these modes is often larger than the typical gyrotron bandwidth, and almost always larger than the spacing between the candidate mode and other possible parasitic modes which couple to the beam as strongly as either of the $TE_{m-1,p}$ or $TE_{m+1,p}$ satellites. This will almost certainly have an effect on the mode competition physics. It has been shown experimentally that this kind of mode competition can be suppressed by a suitable choice of magnetic field and beam radius (Kreischer and Temkin, 1987). As the magnetic field was varied, the gyrotron jumped from one such mode to the neighboring one, but always oscillated stably in a single mode. Which form of mode competition is more important in a given situation depends on the mode spectrum under consideration, and the relative beam–field couplings of neighboring modes. Here, we limit the discussion to competition between two modes with amplitude interaction. The theory of phase interaction is discussed by Nusinovich (1986), .

The efficiency of a single mode can be found by examining the energy balance:

$$d\gamma/dt = e/m_e c^2 \, \vec{E}\cdot\vec{v} \, .$$

Since the electric field is the sum of the eigenfields $\vec{E}_j$, the total change in γ can be expressed in terms of the sum of changes in γ_j. For the efficiency in one mode, we therefore obtain

$$d\gamma_j/dt = e\vec{E}_j\cdot\vec{u}/m_e c\gamma \quad .$$

Using the usual Ansatz for the transverse momentum, $u_x + iu_y = iu_t \, e^{i\Psi}$, and the fact that $\vec{a}_j = -e/m_e c \, \vec{E}_j$, we obtain

$$d\gamma_j/dt = u_t/c\gamma \, [-a_{jx}\sin\Psi + a_{jy}\cos\Psi \,] = (u_t/\gamma)\, du_{jt}/dt. \qquad (29)$$

The efficiency for extraction of energy from the beam to the j'th mode is then

$$\eta_j = (\gamma_0 - \gamma_j)/(\gamma_0 - 1) \, . \qquad (30a)$$

In practice, η_j is calculated by means of an integral over the beam–field interaction:

$$\eta_j = \mathrm{Im}\left[\int_{z_{in}}^{z_{out}} P(z)\, \tilde{F}_j(z)\, (\hat{f}_j(z) e^{i\psi_j})^* \, dz \right] / [u_{z0}(\gamma_0 - 1)] \qquad (30b)$$

A useful check on the numerical accuracy of the calculations is made by showing that $\eta_1+\eta_2 = (\gamma_0 - \gamma)/(\gamma_0 - 1)$, where η_1 and η_2 are calculated as above and γ is given by the total electron energy at the end of the resonator.

Averaging procedure

Eq (30) gives the efficiency for a single electron. This depends on the initial gyrophase Λ_0 of the electron and on the initial phase $\psi_0 = (\omega_{mp} - s_{mp}\,\omega_a)t_0 + (s_{mp} - m)\theta_e$. One must average over the initial uniform distribution of gyrophases and over the initial relative phase of the two modes. The average over gyrophases is performed exactly as in the single mode case. For the average over ψ_0 there are several possibilities.

If $s_1 - m_1 \neq s_2 - m_2$, then one assumes that the electrons are uniformly distributed in azimuth θ_e. The result is independent of assumptions about the value of t_0, the time at which the electrons enter the interaction region. For sufficiently large values of $\Delta\omega = \omega_1 - \omega_2 - (s_1 - s_2)\omega_a$, averaging over the initial beat phase $\Delta\omega t_0$ gives identical results, as has been shown by Nusinovich. The conditions under which averaging over initial beat phase is valid have been discussed by Dialetis and Chu (1983) and by Vomvoridis (1982). Let W_j be the energy stored in the j'th mode. The field amplitude of this mode will not change much during one beat period ($=2\pi/\Delta\omega$) provided that $\eta_j P_{beam} << \Delta\omega\, W_j$. Here $\eta_j P_{beam}$ is an estimate of the energy transferred to the j'th mode during one beat period. For a stationary state, $\omega_j W_j \simeq \eta_j P_{beam} Q_j$. The condition for the averaging over initial beat phases to be correct is that $\omega_j/Q_j << \Delta\omega/2\pi$. The beat period should also not be significantly smaller than the electron transit time through the resonator. If these conditions are fulfilled, numerical results calculated with either averaging method will be identical. The average over θ_e has the advantage that it always works, even for competition between corotating and counter–rotating modes (which have the same frequency in the cold cavity approximation and frequency differences of about $\omega/1000$ when frequency pulling is taken into account). Neither method will work when studying the difference between modes differing only in axial index, such as the TE_{mp1} and TE_{mp2} modes. In typical gyrotrons designed to operate at 140 GHz, $\Delta f \simeq 1$ GHz and $\omega/Q \simeq 3\ ns^{-1}$ for the TE_{mp2} mode. In this case a more detailed analysis, taking time dependence into account must be performed.

We now investigate some applications in the cold cavity, fixed field approximation.

The dynamics and time behavior of two interacting modes is described by the power balance equation

$$Q_j/\omega_j \, dP_j/dt = \eta_j(P_1,P_2)\, UI - P_j \,, \; j=1,2. \tag{31}$$

Here η_j is a function of the amplitudes of the two modes which are assumed to be oscillating (recall that the output power is, at least in the cold cavity, fixed field approximation, proportional to the square of the field amplitude). The time dependence of the beam parameters is neglected here, since these vary much more slowly than either the electron transit time or the cavity reaction time. For the KfK gyrotron, the voltage rise time is typically about 100 μs. Equilibrium is reached when $dP_j/dt = 0$ for both modes. It is possible, and in fact probable, that this equilibrium is achieved for either P_1 or P_2 equal to zero (single mode operation). In many cases two equilibria, corresponding to either of the two modes under consideration, are theoretically possible. In this case, further investigation is needed in order to determine which mode is actually excited. This will be discussed later.

In the cold cavity, fixed field approximation, several questions can be investigated with this formalism. These have been discussed in detail by Jödicke (1989).

The basic method is to take the field profiles, resonant frequencies and quality factors for the two modes of interest for a given resonator geometry, and in principle arbitrary values of amplitude (hence output power) for each mode (the choice of input will be chosen by the physics). If either P_1 or P_2 is zero, the calculation is equivalent to a single mode calculation. We assume that this is not the case. One then solves (28) for given beam parameters to obtain the efficiencies $\eta_j(P_1,P_2)$, j=1,2.

A first application is to determine whether an oscillating mode is stable with respect to perturbations by a parasitic mode. For this, it suffices to calculate the starting current of the parasitic mode 2 in the presence of the first mode:

$$I_{st2} = \lim_{P_2 \to 0} P_2/U\eta_2(P_1,P_2), \tag{32}$$

assuming $P_1 > 0$. If I_{st2} is greater than the beam current I, with

$$I = P_1/U\eta_1(P_1,0) \,,$$

then the first mode oscillates stably. A more detailed justification for this will be given below.

Fig. 6.1 shows the starting current I_{st2} of the TE_{231} mode, calculated assuming that the TE_{031} mode is oscillating, as a function of beam current $I \simeq I_1$. The point O is the limit

for $P_1 \to 0$, and corresponds to the starting current of the TE_{031} mode. The power P_1 increases as the curve is traversed. The line $I = I_{st2}$ separates the region in which the TE_{03} mode is stable from that in which it is unstable.

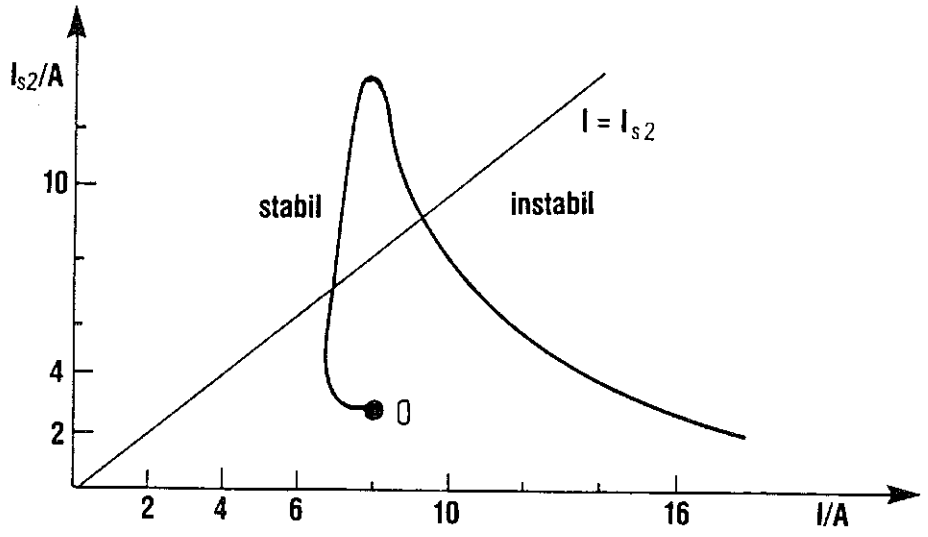

Fig. 6.1. Stability calculation. The amplitude of mode 1 increases along the curve starting at O. If $I_{st2} < I_1 \simeq I$, then mode 1 is unstable with respect to perturbation by mode 2. If $I_{st2} > I$, then mode 1 is stable.

If one now plots the intersection of the two curves as a function of magnetic field, one obtains Fig. 6.2. We have chosen a resonator geometry with $\vartheta_2 = 0.05^\circ$ and $L_2 = 19$ mm. For operation in the TE_{03} mode at 150 GHz, the cavity radius is 3.24 mm and the beam radius is 1.7 mm (second radial maximum). The beam voltage was 70 kV and $\alpha = 1.5$. The TE_{03} mode is stable in the hatched region. In order to determine what happens in the other regions, the dynamics of a two mode system must be considered (see below). Also, the stability region of the competing TE_{23} mode must be investigated. One finds a considerable

region of overlap. In fact, the TE_{23} mode was stable against perturbation by the TE_{03} mode over most of the region in which oscillation was possible (current larger than the minimum current).

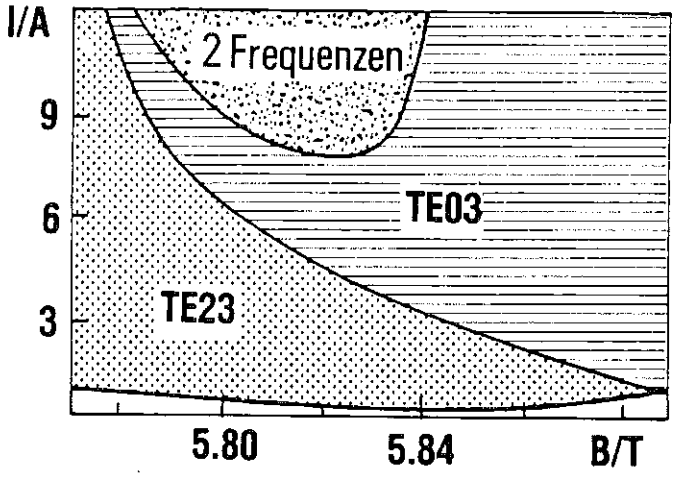

Fig. 6.2. Zones of stable oscillation when the TE03 mode was present first. If the TE23 mode was present first, it oscillates stably over almost all of the shaded region.

In a somewhat different representation of these results, Fig. 6.3 shows the regions in which the $TE_{10,4-}$ and $TE_{7,5+}$ modes can oscillate stably as a function of B/γ_0 and pitch angle when the beam is placed on the first radial maximum of the $TE_{10,4-}$ mode and the current is 20 A. The situation is very similar to competition between the $TE_{0,3}$ and $TE_{2,3}$ modes. We have chosen a resonator geometry with $\vartheta_1=5^\circ$ and $L_2=11$ mm. For operation in the $TE_{10,4}$ mode at 140 GHz, the cavity radius is 8.11 mm and the beam radius is 3.65 mm (first maximum of the corotating component). The results are similar for other mode pairs, provided similar values of dimensionless parameters are considered. There is a considerable region of overlap, especially in the parameter region of interest for high power operation of the $TE_{10,4-}$ mode. This is one limitation of a simple stability analysis. Even if a saturated single mode is found to be stable against small perturbations by other modes, there is no guarantee that the system will evolve from the original conditions to this state.

This type of analysis can also be performed with the field profile of the oscillating mode taken from a self–consistent calculation. Typically, the regions of stability are enlarged, due to the distortion of the field profile at high current and/or high magnetic field as a result of overbunching.

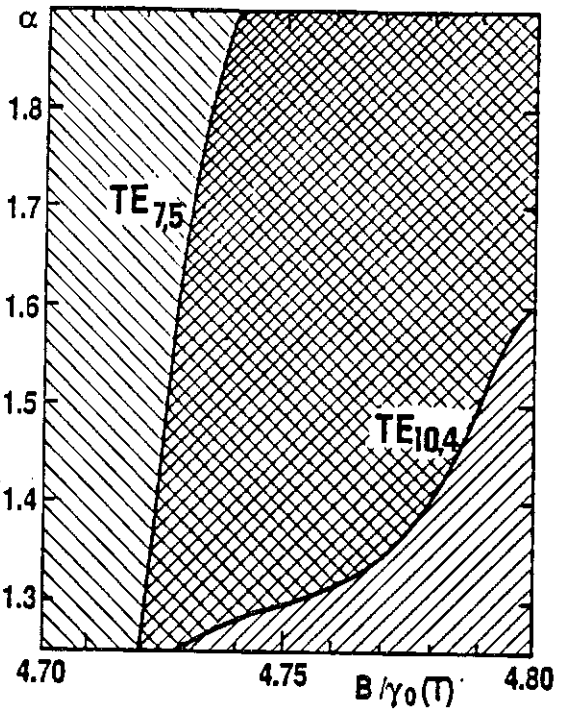

Fig. 6.3. Regions of stability of the TE10,4$^-$ and TE7,5$^+$ modes as a function of magnetic field/γ and α for a resonator in a proposed KfK experiment. The beam is placed on the first radial maximum of the TE10,4$^-$ mode. Accelerating voltage is 80 kV and I = 20 A. The stability regions of the TE7,5$^+$ and of the TE10,4$^-$ modes are indicated by the different directions of hatching. In the cross hatched region whichever mode starts first can oscillate stably once the point of stable equilibrium has been reached.

The limit $P_2 \to 0$ can be taken analytically by linearizing the theory for mode 2 (Borie and Jödicke 1988, Dumbrajs et al 1988). The linearized theory has the advantage that the average over beat phases can be performed analytically. However, this can give rise to numerical problems. The working mode whose stability is to be investigated must be treated numerically. This means that the calculation of $I_1 \simeq I$ is subject to numerical uncertainties.

Fig. 6.4 shows a typical dependence of the efficiency η on output power P (equivalently on the dimensionless amplitude $|F|$) in a single mode calculation. The irregularities in the curve are due to numerical uncertainties and would be ignored in a single mode calculation. They can be explained as follows:

The efficiency of energy transfer by a single electron is a function of initial gyrophase; a typical example of the dependence is shown in Fig. 6.5. Most of the electrons lose energy to the RF field, but a few gain energy. The range of Λ_0 in which the electrons are accelerated is typically quite small, and depends on the amplitude of the RF field. For a

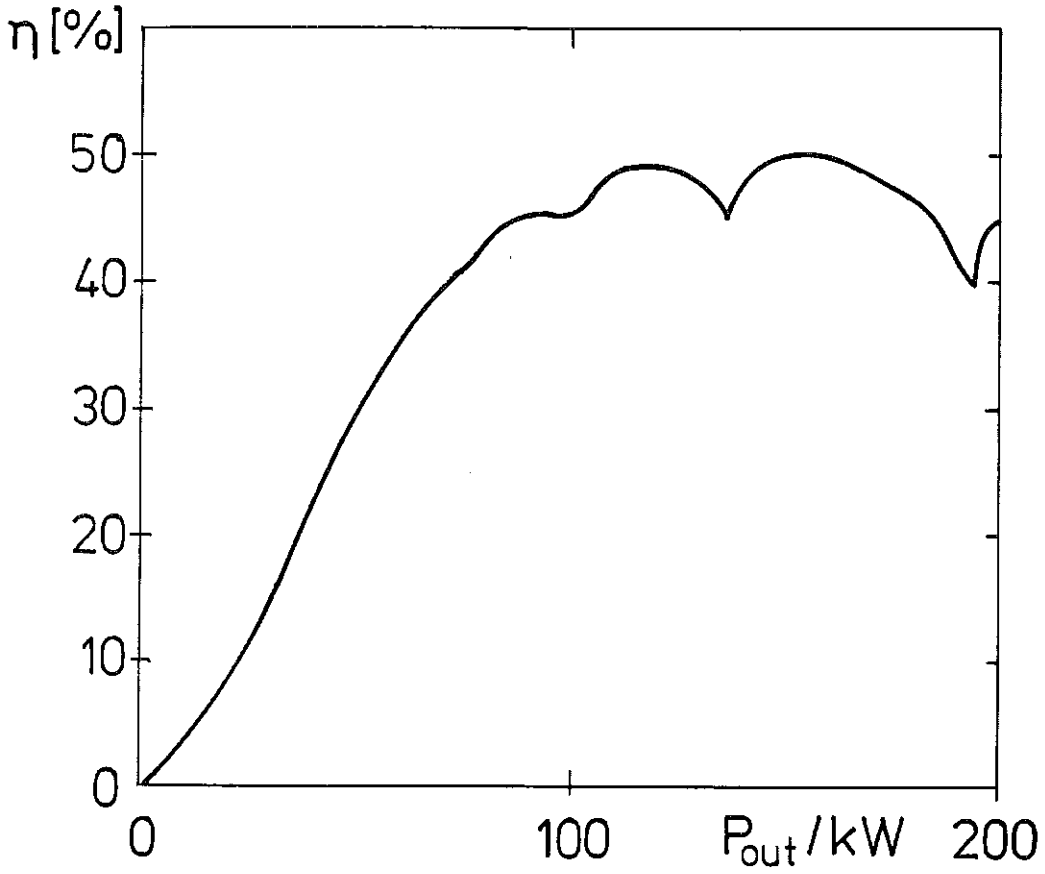

Fig. 6.4. Efficiency of the TE03 mode as a function of output power for a resonator with a slightly tapered midsection and length 19 mm. U=70 kV, α=1.5, B=5.84 T. This calculation was performed with 24 initial gyrophases. The small dips are due to numerical uncertainties and their location depends on the number of initial gyrophases.

numerical average, a finite number of integration points is used. Sometimes the range of Λ_0 in which the electrons have a large negative efficiency contributes very little, and sometimes more than normal. This gives rise to the irregularities in the plot of η vs P. The irregularities are reduced somewhat if a significantly larger number of gyrophases is used, but they never disappear completely. In a single mode calculation, one would simply draw a smooth curve through the points and consider the deviations to be within the numerical uncertainties. If a second mode is assumed to be present with small amplitude, it can happen that the numerical uncertainties in the single mode calculation are more important than the effect of the second mode. To avoid this problem, the limit $P_2 \rightarrow 0$ must be performed very carefully.

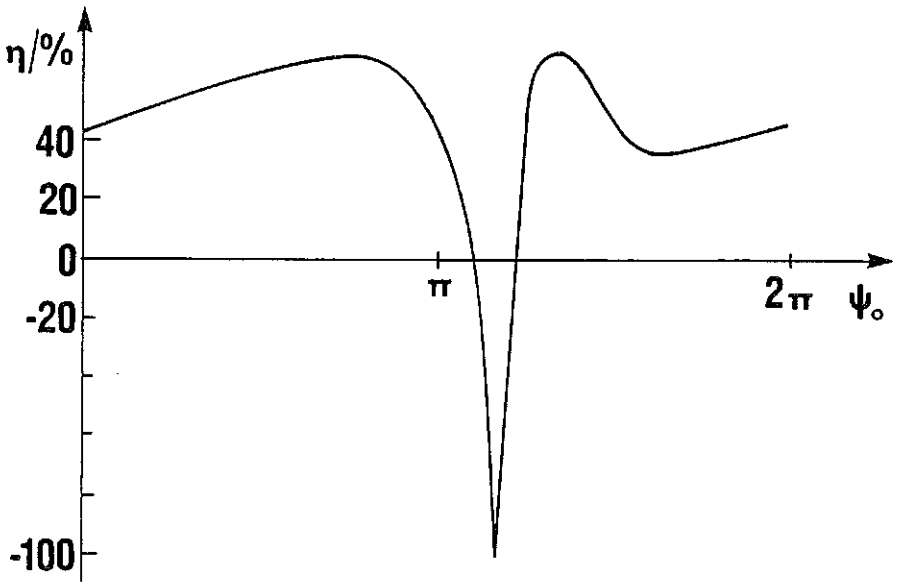

Fig. 6.5. Dependence of efficiency of a single electron on initial gyrophase. The location of the narrow region of negative efficiency depends on beam parameters and field amplitude.

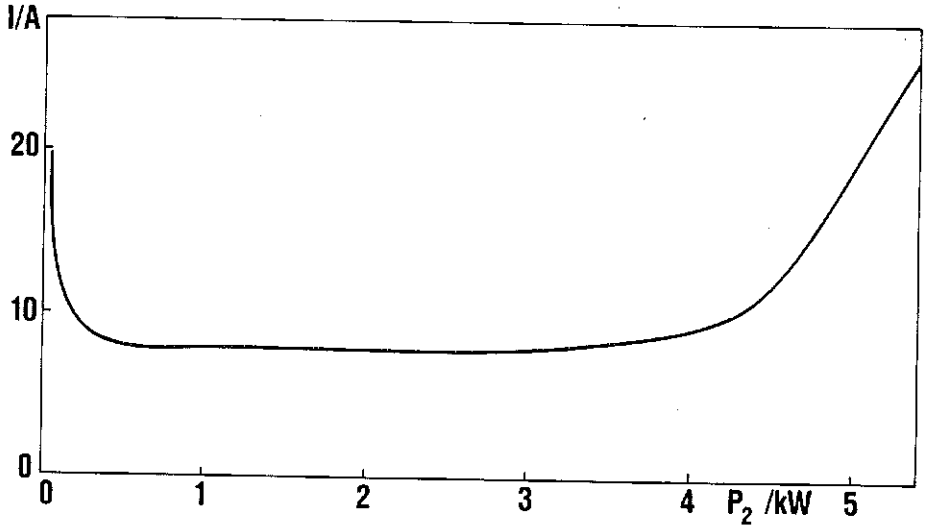

Fig. 6.6. Current I_2 of the TE23 mode as a function of its amplitude (equivalently output power) in the presence of a TE03 mode oscillating at large amplitude (here corresponding to output power 300 kW) The starting current of the TE23 mode is the limit of I_2 for $P_2 \to 0$.

Fig 6.6 shows the current

$$I_2 = P_2/U\eta_2(P_1,P_2),$$

for a fixed output power (P_1 = 300 kW) as a function of P_2. For 0.3 kW < P_2 < 3 kW (0.001 P_1 < P_2 < 0.01 P_1), I_2 is nearly independent of P_2. When P_2 > about 4 kW, nonlinear effects result in a deviation of I_2 from the behavior I_2=const. If P_2 is too small, in this case P_2< 0.3 kW (0.001 P_1), the numerical effects mentioned above become apparant. The truly linear portion of the curve (with I_2=const) would continue to P_2=0, if the numerical noise associated with the calculation of the working mode did not play a role. This constant value is thus the true starting current for the parasitic mode. We now compare the stability region of the TE_{03} mode against perturbation by the TE_{23} mode calculated with the linearized theory (or, equivalently with $P_2 \simeq 0.1$ kW, which gives essentially the same results) and with P_2=1 kW. Fig 6.7a shows the stability region of the TE_{03} mode as a function of magnetic field and current. In the linearized theory, the stability region displays a comb–like structure which is evidently due to the numerical effects discussed above, and hence unphysical. The structure is correlated with the irregularities in the curve of η vs P for the operating mode and depends on the number of simulation electrons. It disappears when the nonlinear theory with P_2=1 kW is used (Fig. 6.7b). The stability region calculated in this manner is essentially independent of the number of averaging electrons, at least as long as enough are used. We shall see below that a mode which oscillates stably according to the criterion described above will quickly suppress a parasitic mode which might happen to start oscillating at a power about 1% of the working mode. Thus, this criterion really is a stability criterion, and can in fact be shown to be equivalent to the one given by Nusinovich (1981, 1986). To recapitulate, in order to calculate reliably the starting current of a parasite in the presence of a working mode while avoiding problems associated with the numerical noise which always accompanies the calculation of the working mode, the amplitude of the parasitic mode, even if this mode is regarded as a small fluctuation, has to be taken in practice to be a little larger than the noise. In practice, one has to take $|F_p\hat{f}_p|^2 \simeq 0.01\ |F_w\hat{f}_w|^2$ (and not less than about $0.001\ |F_w\hat{f}_w|^2$). Results of mode competition calculations obtained using the linearized version of the theory may not be numerically reliable.

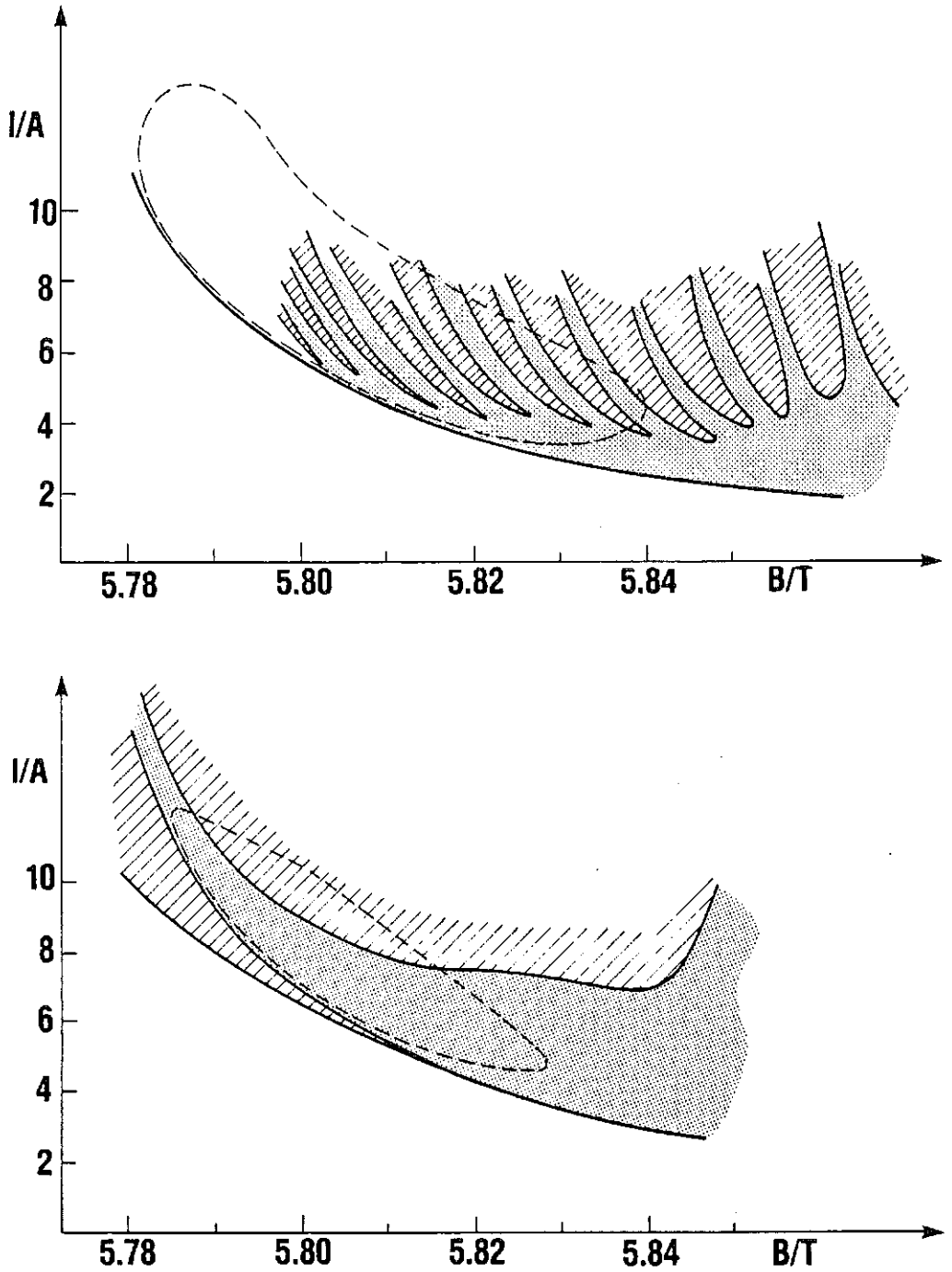

Fig. 6.7. Region of stability of the TE03 mode against perturbation by the TE23 mode calculated for the 19–mm resonator of the KfK experiment. The solid line corresponds to the minimum current of the TE031 mode. The dashed contour shows the contour of electronic efficiency = 50%, calculated in cold cavity, fixed field approximation. Oscillation is stable in the shaded region and unstable in the hatched region. (a) The competing TE231 mode is linearized. (b) The starting current is calculated by taking the limit of the nonlinear theory to low amplitude of the TE23 mode, here corresponding to 1 kW output power.

Dynamics of a two mode system

If the parasitic mode can oscillate, the full nonlinear two mode theory must be used to calculate the stable solution. Equilibrium is attained when

$$I = P_1/U\eta_1(P_1,P_2) = P_2/U\eta_2(P_1,P_2).$$

The dynamics and time behavior of two interacting modes is described by the power balance equation (31), above.

It is a reasonable approximation to assume that the fields do not change significantly during the time an electron travels through the interaction region. Then P_1 and P_2 can be taken approximately constant in the solution of (28) for the η_j. The time development of P_1 and P_2 is then calculated from the power balance equation (31) until either equilibrium is reached or one mode disappears.

For numerical examples, we show results calculated for the $TE_{10,4-}$ mode competing with the $TE_{7,5+}$ mode, as can be expected in a proposed KfK experiment. The situation is very similar to competition between the $TE_{0,3}$ and $TE_{2,3}$ modes. We have chosen the resonator geometry discussed previously in connection with Figs. 2.2, 4.2, 4.3 and 6.3.

Mode suppression:

We next investigate the question of whether the presence of an oscillating mode can suppress the startup of the second mode. At the operating point B=5.52 T, I=20 A, α=1.8, U=80 kV, both the $TE_{10,4}$ and $TE_{7,5}$ modes can oscillate stably according to the theory developed up to now. If one investigates what happens when one mode oscillates with the power predicted by single mode theory and only a small amount of power is in the second mode, one finds that the presence of a stable, oscillating mode suppresses the parasitic mode. Typical time development is shown in Fig. 6.8. Thus, for these parameters, the mode which starts to oscillate first will suppress the other one. This phenomenon has also been discussed by Nusinovich and co–workers (Nusinovich, 1981, Flyagin and Nusinovich, 1986). Thus, there are indeed two stable equilibria, one corresponding to the $TE_{10,4}$ mode and the other to the $TE_{7,5}$ mode. Whichever mode is established first will suppress the other. It becomes more probable that the $TE_{10,4}$ mode will be the operating mode at higher values of B/γ and lower values of α. Similar results for competition between the $TE_{0,3}$ and $TE_{2,3}$ modes have been obtained both theoretically and experimentally (Jödicke, 1989). We repeat that

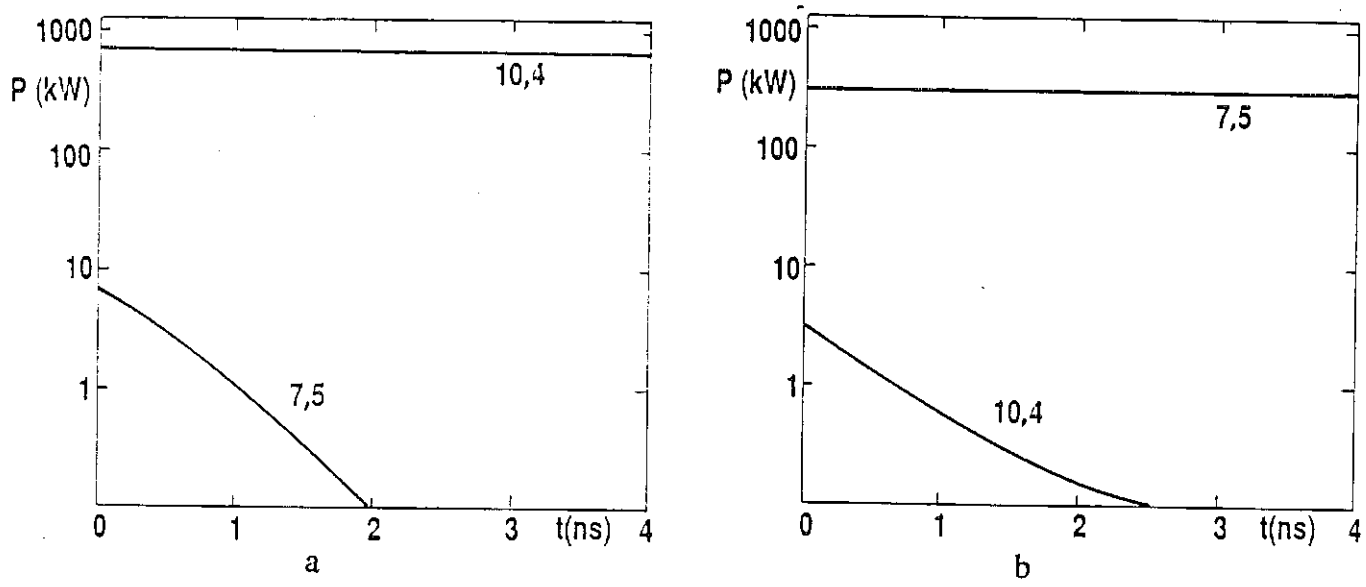

Fig. 6.8. Gyrotron dynamics. Output power vs time for B=5.50 T, U=80 kV, α=1.5 and I=20 A. (a) TE10,4 mode present first. (b) TE7,5 mode present first.

since this kind of mode suppression almost always takes place when $I_{2st} > I_1$, the stability analysis described above is really equivalent to the question of whether a parasitic mode will start or not. Even if it were to oscillate at low power, it would be quickly suppressed. Since the method described here is numerically more reliable, there is no good reason to use a formalism in which the parasitic mode is linearized.

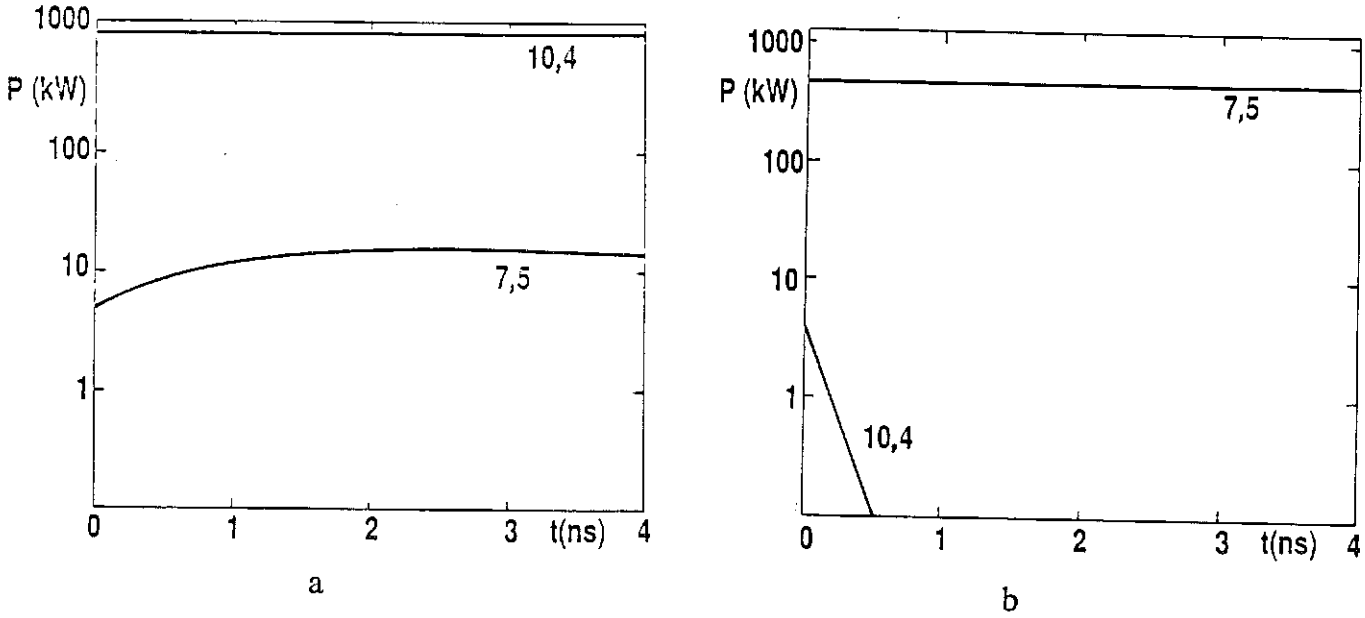

Fig. 6.9. Gyrotron dynamics. Output power vs time for B=5.52 T, U=80 kV, α=1.8 and I=35 A. (a) TE10,4 mode present first. (b) TE7,5 mode present first.

For other parameters, the second mode is not suppressed. One of two things can happen. Either the competing mode is excited and both oscillate (multimoding) or the second mode is excited sufficiently strongly that it suppresses the first mode. Multimoding is most likely to occur for high currents and high values of α. Typical time development is shown in Fig. 6.9a. Here, if the second mode is excited first, it operates stably (Fig. 6.9b). At lower magnetic fields and/or lower currents, the $TE_{10,4}$ mode is unstable. A parasitic mode can be excited and will suppress the oscillating mode.

Influence of time dependence of beam parameters on mode competition

One can control which mode is excited by a suitable startup scenario (Flyagin et al, 1984, Borie and Jödicke, 1987, Dialetis and Chu, 1983, and Levush and Antonsen, 1990). For given beam parameters, modes with a range of detunings are possible single mode equilibria. Which of these is reached depends on the time history of the detuning (basically the voltage rise) and of the other beam parameters ($\beta_\perp$, beam current), as well as on the noise level. If all the parameters were to instantly achieve their final values and the noise level is low, then the mode with the largest linear gain (lowest starting current) grows fastest and suppresses its neighbors. This is shown as the dashed curve in Fig. 6.10. However, if

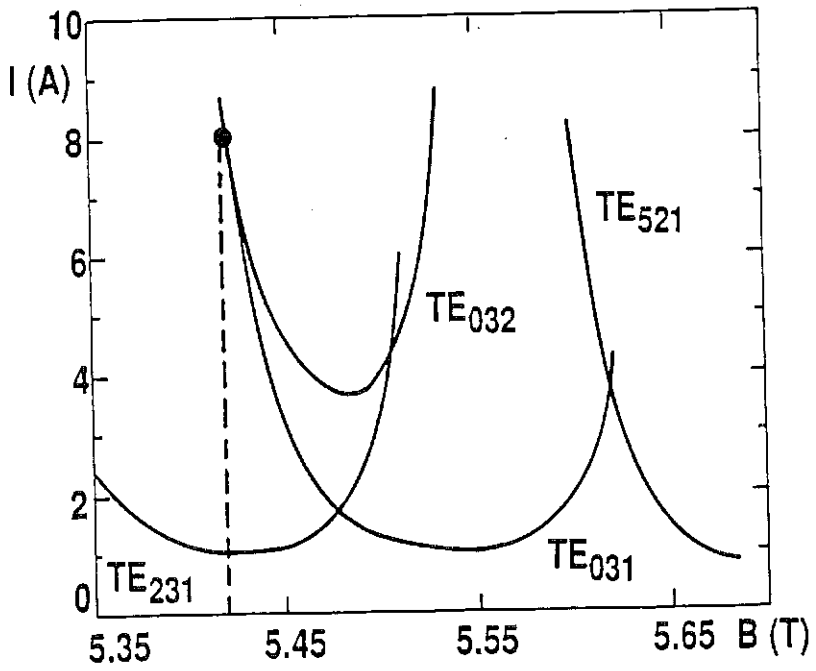

Fig. 6.10 Starting current for the TE_{031}, TE_{032}, TE_{521}, and TE_{231} modes as a function of magnetic field for the 10 mm resonator, assuming beam voltage of 70 kV and $\beta_\perp \simeq 0.4$. The dashed line indicates the startup curve for the case that all beam parameters reach their final values instantly.

the system parameters attain their final values on a time scale long compared with the cavity reaction time Q/ω then the device is likely to pass through a sequence of "mode hoppings". The calculational procedure is then (from Dialetis and Chu, 1983) as follows:

1. Determine the sequence of beam parameters U_b, I_b, $\beta_{\perp 0}$ (hence γ_0 and detuning) taken as the pulse rises. This is illustrated below for the KfK gyrotron.

2. For each set of these parameters, determine the single mode equilibria (starting current and dP/dI (recall that the single mode equilibrium is unstable if $dP/dI < 0$, corresponding to I less than the minimum current). From this, determine which mode, if any, is excited and when. In the following, this is mode 1.

3. Compute the output power, field energy, etc of mode 1 at various points along the trajectory $U_b(t)$, $I_b(t)$, $\beta_{\perp 0}(t)$, as well as its stability against perturbation by mode 2, in the presence of mode 1. If mode 1 becomes unstable, use the power balance equation to find what happens and determine the new equilibrium.

4. Continue this procedure, including a third mode, if necessary, until the final state has been reached.

Typically, the mode with the lowest power threshold will be excited first. As the beam parameters approach their final values, another mode can be excited; however, its threshold must be determined in the presence of the oscillating mode, and is not that given by a single mode starting current calculation. Thus, the starting current curves can provide useful information as to which mode is likely to be excited first, but do not help in determining whether or not the mode remains stable when the large amplitude regime is reached. Most of the time, the system passes through a sequence of stable steady states ("thermodynamically adiabatic" startup). If and when one of these becomes unstable with respect to perturbation by a parasitic mode, the system jumps to a different stable steady state. The final state is usually dominated by a single stable steady state. It suffices to consider about ten points on the voltage rise curve.

We illustrate this with a specific example, here corresponding to recent experiments at KfK at 140 GHz. Fig. 6.11a shows $\beta_\perp(t)$, and Fig. 6.11b shows $\alpha(t)$ for a voltage rise time of 190 μs, assuming that the beam voltage and mod anode voltage are coupled by an ohmic divider (solid curve in 22b). Thus U and $\beta_\perp$ are proportional to time. Here the final values are U=70 kV, $\beta_\perp$=0.4, α=1.5 and I=8 A. The dashed curve in Fig. 6.11b is the value of α when the beam voltage is constant and only $\beta_\perp$ varies with the mod anode voltage.

Fig. 6.11c shows the output power as a function of time, including the mode which oscillates, for the 10 mm resonator used in the KfK experiments at 140 GHz. The detailed geometry has been described in Sect. II. Here the magnetic field is chosen to be 5.42 T. The

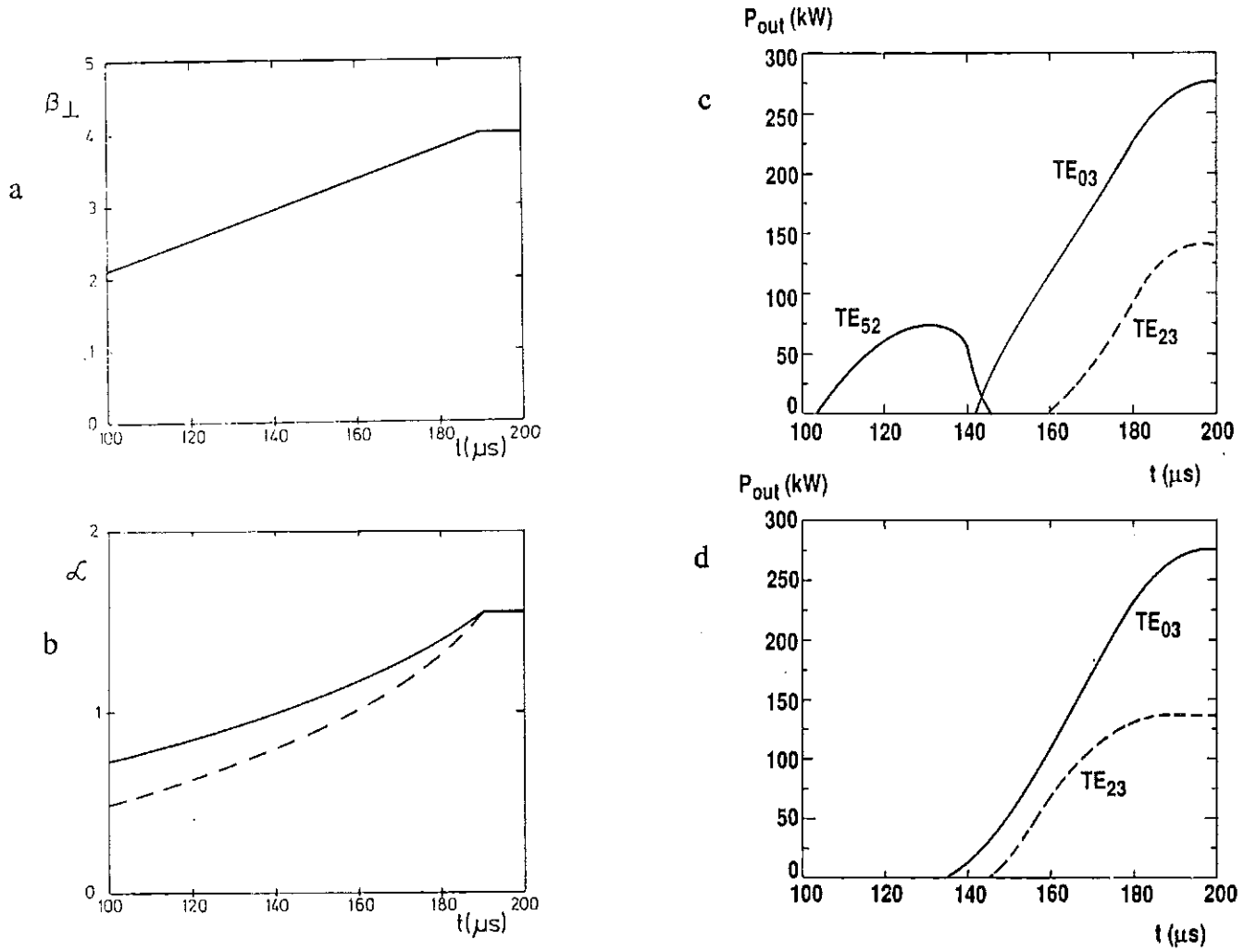

Fig. 6.11. Time dependence of $\beta_\perp$ (a) and velocity ratio α (b) for two different startup scenarios. The solid curve in (b) corresponds to accelerating voltage and mod anode voltage connected by an ohmic divider and the dashed curve to accelerating voltage fixed, mod anode voltage pulsed. The rise time is 190 μs. (c), (d): output power in the TE_{52}, TE_{03} and TE_{23} modes as a function of time c) accelerating voltage and mod anode voltage connected by an ohmic divider. d) accelerating voltage fixed, mod anode voltage pulsed.

frequencies of the TE_{mp1} modes are: mp=03, f=140.22 GHz; mp=52, f=144.98 GHz, mp=23, f=137.42 GHz. At t≃110 μs, the TE_{52} mode starts, reaches a maximum power of about 75 kW at t≃130 μs, and then decreases in power as the detuning becomes less favorable. At t≃142 μs, the TE_{03} mode can start, and then quickly suppresses the TE_{52} mode, which by then is nearly unstable in a single mode calculation anyway. The TE_{03} mode remains stable against perturbation by the TE_{23} mode, which, in the absence of a TE_{03} mode, would start to oscillate at t≃160 μs and reach a final output power of 137 kW. The situation is somewhat different when the accelerating voltage is held constant at 70 kV and only the mod anode voltage is pulsed (Fig. 6.11d). In that case the TE_{03} mode starts at 140 μs and is stable against perturbation by a parasitic TE_{23} mode. If the TE_{03} mode were not present, the TE_{23} mode would start at about 150 μs. If one examines the starting current curves at constant α, one would expect the TE_{23} mode to start first (fig. 6.10). The fact that this is not the case is due to the variation in α. Fig. 6.12 shows the starting current for the two modes as a function of α for B=5.42 T and U=70 kV. Although the minimum starting current of the TE_{23} mode is much lower, there is a range of $\alpha < 1$ for which the starting current of the TE_{03} mode is lower than that of the TE_{23} mode. An experimental application of this procedure was given by Jödicke (1989).

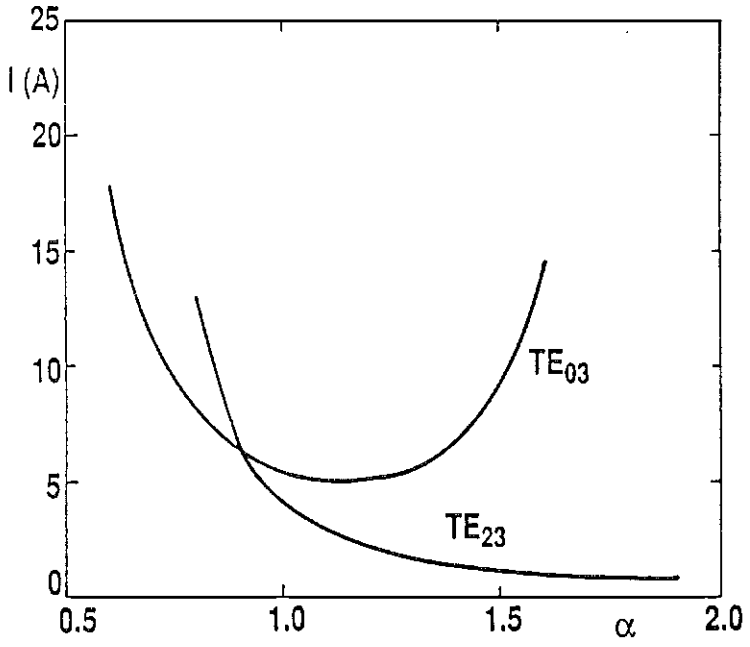

Fig. 6.12. Starting current for the TE_{031} and TE_{231} modes as a function of velocity ratio α for the 10 mm resonator, assuming beam voltage of 70 kV and B = 5.42 T.

In gyrotrons the electron beam radius R_e is usually chosen such as to maximize the coupling of the electron beam to the RF field which is polarized either corotating or counter–rotating with respect to the gyrating electrons ($|J_{m\pm1}(k_{mp}R_e)|$ is maximum). Sometimes the beam radius has some other value, for various reasons, especially in a step tunable gyrotron, since the magnetic field is varied over a wide range and the beam radius is related to the magnetic field by $R_e = R_c\sqrt{B_c/B_0}$ where R_c= cathode radius and B_c is the cathode magnetic field. In such a situation, the coupling of the beam to both rotating RF field components may become comparable. It was shown a long time ago by Moiseev and Nusinovich (1974) that if the beam–field coupling coefficients differ by as little as 10%, the polarization component with the strongest coupling to the beam will suppress the other. This has been confirmed by calculations performed with the present formalism. We consider a resonator designed to operate in the $TE_{15,2}$ mode at 140 GHz, corresponding to experiments performed at MIT (Kreischer et al 1990) and by Varian (Felch et al, 1990). The cavity radius is R_0 = 7.53 mm, and the resonator mid section is 7 mm long. The frequency of the $TE_{15,2,1}$ mode is 140.84 GHz and the quality factor Q=409. We consider the case B=5.52 T, α=1.8, I=35 A, U =80 kV, and varied the beam radius from 5.3 mm to 5.9 mm. R_e=5.4 mm corresponds to the first radial maximum of the corotating component, and R_e=5.9 mm corresponds to the first radial maximum of the counterrotating component. We consider two methods of calculation:

i) Both modes in cold cavity, fixed field approximation. Assume one component is oscillating with power 1000 kW (close to the result of a single mode calculation with beam on the appropriate radial maximum) and the other with an amplitude corresponding to 1% of this power. Look for equilibrium.

ii) Calculate one component self–consistently and examine its stability with respect to perturbation by the other component, considered as a parasite. The latter is calculated in cold cavity approximation.

Table 2 shows $|J_{m\pm1}(k_{mp}R_e)|$ as a function of R_e. These differ by less than 10% only for R_e = 5.7 mm and 5.8 mm. The cold cavity calculations (method (a)) confirmed the old result of Moiseev and Nusinovich (1974), namely that for $R_e \leq 5.6$ mm, the corotating polarization will oscillate, no matter what the relative starting amplitudes. If $R_e \geq 5.9$ mm, then the counter–rotating polarization will oscillate. For the other parameters as used here, the beam current parameter I_{mp} was less than the minimum value for $|G_{mp}| \leq 0.21$ and no self–consistent single mode solution was found. Thus, for these values of R_e, method (b)

gave the same results, except that the single mode efficiency and output power differed somewhat between the cold cavity and self–consistent calculations. For R_e = 5.7 mm, the cold cavity calculation indicated that the corotating polarization would oscillate alone if it started first (with power about 1100 kW), whereas multimoding with P_+=700 kW and P_-=10 kW could occur if the counter–rotating component started first. If the working mode was calculated self–consistently, it was stable against perturbation by the other polarization component. The situation is similar for R_e = 5.8 mm, except that the counter–rotating polarization could oscillate alone in cold cavity approximation. Stability analysis treating also the parasitic mode self–consistently has not been undertaken. Clearly it is only of interest for a very narrow range of beam radii.

Table 2. $|G_{mp}|$ as a function of beam radius for the corotating and counter–rotating polarizations of the $TE_{15,2}$ mode.

R_e (mm)	$\lvert J_{m-1}(k_{mp}R_e)\rvert$	$\lvert J_{m+1}(k_{mp}R_e)\rvert$
5.3	.268	.152
5.4	.272	.170
5.5	.271	.189
5.6	.264	.206
5.7	.251	.223
5.8	.232	.237
5.9	.206	.249
6.0	.175	.247

We now consider the modifications to the theory when the field equations for each mode take into account the effect of the beam in a self–consistent calculation of mode competition. The derivation has been given elsewhere (Jödicke 1989, Borie and Jödicke 1991) and we will not repeat it here.

The self–consistent system of equations for mode competition are, in terms of the dimensionless variables described in Sect. V ($\hat{f}_{mp}$ is the field profile normalized to $|\hat{f}|_{max}$=1).

$$d\tilde{P}/d\tilde{z} + i\,(\gamma/\gamma_0 - 1 + \delta)\,\tilde{P} =$$
$$= i\,\gamma/\gamma_0 \,\Sigma\, F_{mp}\,\hat{f}_{mp}(z)\,\exp(i(\omega_{mp} - \omega_a)t + i(1-m)\theta_e) \qquad (33)$$

and

$$[d^2/d\tilde{z}^2 + \beta_{z0}^2 (\omega_{mp}^2 - c^2 k_{mp}^2(\tilde{z}))/\omega_a^2 + I_{mp}] F_{mp} \hat{f}_{mp}$$
$$= -I_{mp} \Omega_0/\omega_a < < \tilde{P}/\gamma > e^{i(\omega_a - \omega_{mp})t + i(m-1)\theta_e>} \qquad (34)$$

where now

$$\delta = 1 - \Omega_0/ \omega_a \gamma_0 , \qquad \tilde{P} = P/u_{t0}, \qquad \tilde{z} = \omega_a z/v_{z0},$$
$$F_{mp} = (eV_{max}/2m_e c^2) (C_{mp} G_{mp})/u_{t0} (ck_{mp}/\omega_a) \text{ and}$$
$$I_{mp} = (eZ_0 I_0/2m_e c^2) \beta_{z0} (C_{mp} G_{mp})^2/\gamma_0 (ck_{mp}/\omega_a)^2 .$$

and the average in (34) is taken over initial gyrophase and ψ_0 , as before.

Since $t = \int \gamma/(\gamma_0 v_{z0}) \, dz = 1/\omega_a \int \gamma/\gamma_0 \, d\tilde{z}$, we have

$$(\omega_{mp} - \omega_a)t = (\omega_{mp}/\omega_a - 1) \int \gamma/\gamma_0 \, d\tilde{z} .$$

The free parameters are δ and I_{mp}, as well as the resonator geometry. These determine ω_{mp}/ω_a and $F_{mp}\hat{f}_{mp}$ (for each mode).

For numerical calculations, the boundary condition at z_{out} is reformulated in the form

$$|R| = |(dV/dz + ik_z V)/(dV/dz - ik_z V)| = \text{minimum (for each mode).}$$

In principle, one could assign a nonzero reflection coefficient to each mode, allowing for a frequency–dependent load. However, the number of free parameters rapidly becomes intractable.

Solutions of this system have up to now been limited to determining the stability of a working mode in the presence of an operating mode. The field profile of the assumed working mode is calculated self–consistently and the stability of this mode with respect to perturbation by a possible parasitic mode is investigated. One tries to find a solution to the equations (33), with mode 1 fixed from the self–consistent single mode calculation and Eq. (34) for the parasitic mode (mode 2). It is possible to investigate whether mode 2 can be present with an amplitude larger than the numerical noise (if not, the working mode is stable), or, analogous to the previous investigation of stability in the cold cavity approximation, by calculating the starting current for the second mode self–consistently in presence of the working mode. It is assumed that the amplitude of the second mode is small, but sufficiently large that the numerical problems associated with the use of the linearized theory do not arise. Typically, one takes $|F_2\hat{f}_2(z=0)|^2/|F_1\hat{f}_1(z=0)|^2$ to be between 0.001 and 0.01. In (34) the beam current I_0 is replaced by I_{2st} and the frequency ω_2 and I_{2st} are

varied until the reflection coefficient for mode 2 is minimized. If I_{2st} is larger than the beam current, one concludes that the parasitic mode cannot start in the presence of the working mode. The results obtained up to now with both methods indicate that multimoding is far less likely to occur in a self–consistent calculation than in the cold cavity approximation. This seems to be due mainly to the changes in the single mode field calculated for the working mode. For some reason, overbunching can make the working mode more stable with respect to perturbation by parasitic modes. A self–consistent calculation of the startup behavior, which could give more information as to which mode actually starts, has not been performed up to now in this type of formalism. It may well suffice to do this calculation in single mode approximation, since the minimum current is the quantity which is most affected by taking into account the effect of the source on the field profile.

Time dependent dynamics for short pulse gyrotrons

We remark that for the time scales typical of gyrotron oscillators, an explicitly time dependent formalism is inappropriate, since numerical stability, determined by the Courant condition (see Hockney and Eastwood, 1981) requires time steps of the order of a fraction of a nanosecond, while the voltage rise times are of the order of at least several microseconds. This restriction does not apply to relativistic, pulse–power gyrotrons. In this chapter, we concentrated on the slow rise time case. The relativistic gyrotron is described well by (Bratman, Petelin, 1981b and by Fliflet (1986) and Fliflet and Manheimer (1989). These devices, based on intense relativistic electron beams (U ≈ several hundred kV, I ≈ several hundred A) are characterized by short pulse lengths (≈ 50 ns) and voltage rise times, and ripple effects which can prevent the establishment of a steady state equilibrium. Startup behavior cannot be analyzed as a sequence of steady states in this case. Experiments have been carried out at NRL (Gold et al 1985, 1987). Simulations of such cases have been described by Lin et al (1988b), using both the slow time scale, single mode approach of Fliflet and Manheimer (1989) and a multimode particle simulation code (Lin et al 1988a). In single mode approximation, both methods gave similar results which were in fairly good agreement with experiment. The onset of high power operation is sensitive to variation of the beam current and α with voltage, which is experimentally not very well known.

The simulation of Lin et al (1988a) assumes fixed transverse (radial and azimuthal) field dependence for each mode, and calculates the polarization, temporal and axial dependence of the fields self–consistently, taking into account the presence of the beam. The

time dependence, density profile and velocity spread of the beam can be realistically modelled. In single mode approximation, with a beam having no velocity spread and all guiding centers at the same radius, the results agreed with those of Fliflet and Manheimer for the same beam parameters. Examination of details of the calculations revealed some interesting further results.

At high currents the field profile rises faster, and energy extraction is earlier, than is the case at lower currents. This may be related to the overbunching sometimes found in steady state calculations. Self–consistency is very important for currents much larger than the starting current. The filling time depends on the ratio I/I_{st} as well as on $2Q/\omega$. The theoretical efficiency is a factor 2 larger than the experimental efficiency, and this is probably due to the effects of space charge and time dependent fluctuations of the voltage pulse.

The time dependence of the field energy can often be briefly described as rapid growth of the field, overshooting of the saturation point, and attainment of a steady state after a few amplitude modulations. These results are at least qualitatively similar to those of Ginzburg et al (1986), who used a nonsteady state particle tracing approach. The modulation can last several hundred wave periods and thus cannot be neglected in short pulse gyrotrons.

If the AC beam current and cavity mode are each decomposed into forward and backward going waves, one finds that each component of the current can interact with each component of the cavity mode, resulting in unequally deposited energy in the two components. These components are separated by wave transit time effects in the gyrotron cavity, which can result in modulation of the emission at the radiation bounce frequency. The degree of such self modulation depends on the degree of unbalanced power deposition and is thus more likely to occur at higher beam currents and/or higher magnetic fields. At sufficiently high currents, evidence for additional modulation at twice the original modulation frequency was found and the system becomes chaotic.

The separate and unequal couplings to forward and backward waves give rise to a more complicated picture of mode competition between closely spaced TE_{m2} modes than a steady state model would predict. In some cases modes which are sufficiently detuned that it should not oscillate can grow to high power. This seems to be a sensitive function of conditions during the rise of the pulse and is probably difficult to observe experimentally for this reason.

VII COMPLEX (STEP) CAVITIES

A complex cavity for a gyrotron was first proposed in 1979 by Pavel'ev and Tsimring. It consists of two resonators I and II, as shown in Fig. 7.1. The concept was experimentally demonstrated in a TE_{01}/TE_{04} configuration by Carmel et al (1983), and has been incorporated in TE_{01}/TE_{02} devices at 60 and 70 GHz (Felch et al, 1984, 1990) and in a 140 GHz TE_{02}/TE_{03} device developed at Varian (Felch et al, 1986b). Operation of step

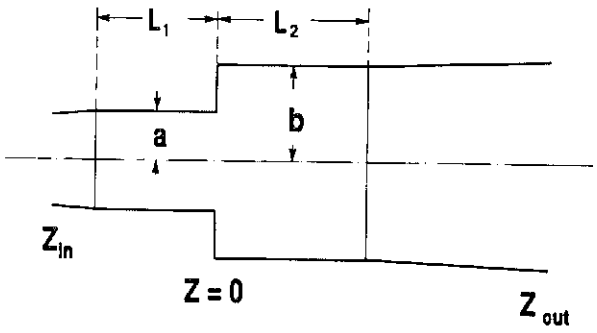

FIG. 7.1. Typical complex cavity. Each of the two uniform sections is close to cutoff for a mode pair having the same azimuthal index m and the same operating frequency.

cavity devices at higher harmonics has been demonstrated by Zapevalov et al (1984) and by Malygin (1986). On the other hand, Thompson CSF has experienced difficulties with a TE02/TE04 complex cavity at 100 GHz (Garin et al 1987) and has decided to work instead with volume modes in simple cavities. The essential idea of this approach is that a pair of modes having the same azimuthal index m and different radial indices can be coupled to produce a high Q mode of the complete cavity. The mode coupling occurs at the sudden change in the cavity wall radius. The cavity is designed such that the local waveguide modes of the desired pair have the same frequency and are simultaneously near cutoff in the

two sections. The two resonators are detuned for other mode pairs. This permits better mode control in a highly overmoded second cavity. In addition, the first cavity may serve to prebunch the electrons in the beam, which can lead to efficiency enhancement. The success of this approach depends on several factors, including mode density, fabrication tolerances, and mode conversion at the cavity step. At sufficiently high mode densities, more than one mode can become simultaneously resonant. Conversion to unwanted modes at the step can degrade the mode purity of the device. Step cavity devices are more sensitive to machining tolerances than conventional gyromonotrons because of the bimodal resonance condition.

The most recent theoretical treatments of complex cavities have been given by Dumbrajs and Borie (1988), Fliflet (1988), Pavel'ev et al (1987), and Nielson et al (1989). The review of Pavel'ev et al surveys the experimental situation, considers particle motion for the case in which the field profiles are Gaussian (one Gaussian in each cavity), and describes a method for calculating the field profiles more exactly. The other authors all calculate the field profiles explicitly, thus including the effect of mode conversion at the transition exactly and permitting a study of the effect of machining tolerances on the performance of the device. Fliflet gives a self consistent calculation, assuming that on either side of the cavity step, the beam interacts with a single TE mode of the form (2). The equations of motion are the same as those given in Sect. 3, including the effect of a possible magnetic field taper. The work of Borie et al (1988) indicates that the approximation used by Fliflet et al for the electron motion is valid. The more exact slow–variables equation of motion (16) was used with the RF fields calculated in two different ways: including all propagating modes and including only the principal modes. The results were essentially identical for a wide range of parameters. This means that the nonresonant propagating modes excited by mode conversion at the step do not contribute significantly to the electron motion.

We must now consider the problem of field matching at the cavity step (for convenience taken to be at z=0). The field is expanded in terms of the eigenfields of the normal modes of the two connecting waveguides:

$$\text{Region I} \quad \vec{E}_t = \Sigma\,(a_{ip} + a_{rp})\,\vec{e}^{\,a}_{mp}$$

$$\vec{H}_t = \Sigma\,(a_{ip} - a_{rp})/Z^a_{mp}\,\vec{h}^{\,a}_{mp}$$

with $\vec{h}^{\,a}_{mp} = \hat{z} \times \vec{e}^{\,a}_{mp}$ and

$Z^a_{mp} = \mu_0\omega/[\omega^2/c^2 - x^2_{mp}/a^2]^{1/2}$ for TE modes and $[\omega^2/c^2 - y^2_{mp}/a^2]^{1/2}/\epsilon_0\omega$ for TM modes.

$$\text{Region II} \quad \vec{E}_t = \Sigma\,(b_{ip} + b_{rp})\,\vec{e}^{\,b}_{mp}$$

$$\vec{H}_t = \Sigma\,(b_{ip} - b_{rp})/Z^b_{mp}\,\vec{h}^{\,b}_{mp}$$

with $\vec{h}^{b}_{mp} = \hat{z} \times \vec{e}^{b}_{mp}$ and

$Z^{b}_{mp} = \mu_0\omega/[\omega^2/c^2 - x^2_{mp}/b^2]^{1/2}$ for TE modes and $[\omega^2/c^2 - y^2_{mp}/b^2]^{1/2}/\epsilon_0\omega$ for TM modes. The subscripts i and r refer to incoming and reflected waves, respectively (or waves propagating forward and backward). The basis functions (including normalization) are the same as in Sect. . Matching the fields at z=0 gives

$$\Sigma\,(a_{ip} + a_{rp})\,\vec{e}^{a}_{mp} = \Sigma\,(b_{ip} + b_{rp})\,\vec{e}^{b}_{mp} \qquad (36)$$

$$\Sigma\,(a_{ip} - a_{rp})/Z^{a}_{mp}\,\vec{h}^{a}_{mp} = \Sigma\,(b_{ip} - b_{rp})/Z^{b}_{mp}\,\vec{h}^{b}_{mp} \qquad (37)$$

Taking the scalar product of (36) with $\vec{e}^{a\,*}_{mp}$ and of (37) with $\vec{h}^{a\,*}_{mp}$ and integrating over the surface gives

$$a_{ip} + a_{rp} = \Sigma\,(b_{is} + b_{rs})\,C_{ps} \qquad (38a)$$

$$a_{ip} - a_{rp} = \Sigma\,(b_{is} - b_{rs})Z^{a}_{mp}/Z^{b}_{ms}\,C_{ps} \qquad (38b)$$

Here $C_{ps} = \int \vec{e}^{\,*a}_{mp} \cdot \vec{e}^{b}_{ms}\,dA$ are coupling coefficients. They have been given explicitly (for the normalization used here) by Neilson et al (1989) for general m and by Dumbrajs and Borie (1988) for m=0. For TE(I)→TE(II):

$$C_{ps} = 2ax_{ms}/b\;J'_m(x_{ms}a/b)/J_m(x_{ms})\;1/[(x^2_{mp}-m^2)(x^2_{ms}-m^2)\,]^{1/2}\;[1 - (x_{ms}a/x_{mp}b)^2\,]$$

TE(I)→TM(II):

$$C_{ps} = 2m/y_{ms}\;J_m(y_{ms}a/b)/J_{m+1}(y_{ms})\;1/[(x^2_{mp}-m^2)]^{1/2} \qquad (39b)$$

TM(I)→TE(II):

$$C_{ps} = 0 \qquad (39c)$$

TM(I)→TM(II):

$$C_{ps} = -2/y_{ms}\;J_m(y_{ms}a/b)/J_{m+1}(y_{ms})\;1/[1 - (y_{mp}b/y_{ms}a)^2\,] \qquad (39d)$$

Both propagating and evanescent modes must be taken into account in the sums. According to Fliflet et al (1988), it is usually sufficient to restrict oneself to a single incident TE_{mP} wave at the input. In Fliflet's code, the self–consistent equations are then integrated up to the cavity step. Only beam interaction with this TE_{mP} mode are included. This integration determines the amplitudes a_{iP} and a_{rP} at the step. The other coefficients must be determined, assuming that $a_{ip}=0$ if $p \neq P$. Assuming that the beam only interacts with a single TE_{mQ} mode for z>0, and that any non–resonant propagating modes excited by mode conversion at the step will simply propagate out of the system without reflection at the

cavity input and output sections, one integrates the equations of electron motion together with the field equation for the TE_{mQ} mode to the cavity end. The boundary condition $dV_{mQ}/dz+ik_z V_{mQ} = 0$ at $z=z_{out}$ determines the frequency and $V_{mP}(z_{in})$, which must be found by a search procedure, as in the self–consistent calculation for a simple cavity.

Published practical examples with realistic field profiles have all dealt with the case m=0. In that case there is no conversion to TM modes at the step. Fliflet et al considered the TE01/TE04 step cavity configuration corresponding to the experiment of Carmel et al (1983). Extensive parameter studies by Borie et al (1988) demonstrated the sensitivity of complex cavities designed to operate at 140 GHz to machining tolerances of the order of 0.01 mm.

This work was performed under the auspices of the Projekt Kernfusion at the Kernforschungszentrum Karlsruhe and supported by the European community as part of the European Fusion Technology Program.

A number of colleagues have participated in the work at KfK described here, especially in the form of help with parameter studies, and programming details. We particularly want to thank H. Wenzelburger, M. Hillmer, O. Dumbrajs, G. Gantenbein, A. Möbius, and R.J. Gupta for their assistance in this respect.

I also express very special gratitude to B. Jödicke, who participated in so many of the calculations whose results are presented here. It would not have been possible to do work of this quality without his constant supply of fresh ideas and new ways of looking at problems. I also want to thank Prof. A. Citron and G. Hochschild for introducing me to this field and for their constant encouragement during the early stages of this work. They were responsible for initiating the KfK gyrotron program.

Finally, I wish to thank M. Thumm, B. Piosczyk, B. Jödicke and G. Gantenbein for stimulating discussions and critical reading of the manuscript.

REFERENCES

Abramowitz, M., Stegun, I.A., 1970. Handbook of Mathematical Functions, New York, Dover Publications. Ch. 9.

Akhizer, A.I., Berestetskii, V.B., 1965. Quantum Electrodynamics (English translation), §12.5, Wiley Interscience, New York.

Andronov, A.A., Flyagin, V.A., Gaponov, A.V., Gol'denberg, A.L., Petelin, M.I., Usov, V.G., Yulpatov, V.K., 1978. The gyrotron: high power source of millimeter and submillimeter waves. Infrared Physics 18, 385–393

Antonsen, T.M., Manheimer, W.M., Levush, B., 1986. Effect of AC and DC self–fields in gyrotrons. Int. J. Electronics 61, 823–854

Antonsen, T.M., Levush, B., 1989. Mode competition in gyrotrons and free electron lasers, 14th Int. Conf. on Infrared and Millimeter Waves, Würzburg.

Baird, J.M., 1987. Gyrotron Theory, in "High–Power Microwave Sources", eds. V.L. Granatstein and I. Alexeff, Artech House, Boston, 1987, Ch. 4.

Barroso, J.J., Montes, A., Silva, C.A.B., 1985. The use of a synthesis method in the design of gyrotron electron guns. Int. J. Electronics 59, 33–47.

Barroso, J.J., Montes, A., Ludwig, G.O., 1986. RF Field Profiles in weakly irregular open resonators. Int. J. Electronics 61, 771–794.

Barroso, J.J., Correa, R.A., Montes, A., 1989. Optimization of RF field profiles for enhanced gyrotron efficiency. Int. J. Electronics 67, 457–484.

Barroso, J.J., Montes, A., Ludwig, G.O., Correa, R.A., 1990. Design of a 35 GHz gyrotron. Int. J. of Infrared and Millimeter Waves 11, 251–274.

Bensimon, A., Faillon, G., Garin, P., Mourier, G., 1984, Gyrotron development at Thomson–CSF, Int. J. Electronics 57, 805–814.

Bernstein, I.B., Divringi, L.K., Smith, T.M., 1983. The theory of irregular waveguides and open resonators. Int. J. of Infrared and Millimeter Waves 3, 57–117.

Birdsall, C.K., 1987. Particle Simulation Techniques for Beam Devices, in "High–Power Microwave Sources", eds. V.L. Granatstein and I. Alexeff, Artech House, Boston, 1987, Ch. 3.

Bondeson, A., Manheimer, W.M., Ott, E., 1983. Multimode analysis of quasioptical gyrotrons and gyroklystrons. Infrared and Millimeter Waves, K. Button, ed. (Academic Press,New York), vol 9, 309–340.

Borie, E., Dumbrajs, O., 1986. Calculation of eigenmodes of tapered gyrotron resonators. Int. J. Electronics 60, 143–154.

Borie, E., Dumbrajs, O., Jödicke, B., 1986. Parameter studies for a 150 GHz gyrotron operating in the TE03 mode. Int. J. Electronics 61, 735–746.

Borie, E., 1986. Self–consistent code for a 150 GHz gyrotron. Int. J. of Infrared and Millimeter Waves 7, 1863–1879.

Borie, E., Jödicke, B., 1987. Startup and mode competition in a 150 GHz gyrotron. Int. J. of Infrared and Millimeter Waves 8, 207–226.

Borie, E., Jödicke, B., Wenzelburger, H., Dumbrajs, O., 1988. Resonator design studies for a 150 GHz gyrotron at KfK. Int. J. Electronics, 64, 107–126.

Borie, E., Jödicke, B., 1988. Comments on the linear theory of the gyrotron. IEEE Trans. Plasma Sci. 16, 116–121.

Borie, E., Dumbrajs, O., Gupta, R.K., Möbius, A., Piosczyk, B., Wenzelburger, H., 1989. KfK internal report, unpublished.

Borie, E., 1989. KfK internal report, unpublished.

Borie, E., Jödicke, B., 1990. Rieke Diagrams for gyrotrons. Int. J. of Infrared and Millimeter Waves 11, 243–250.

Borie, E., Jödicke, B., 1991. Self–consistent theory of mode competition in gyrotrons. to be published .

Boucher, G., Boulanger, Ph., Charbit, P., Faillon, G., Herscovici, A., Kammerer, E., Mourier, G.,, 1983. A Gyrotron Study Program, Infrared and Millimeter Waves 9, 283–308.

Bratman, V.L., Moiseev, M.A., Petelin, M.I., Erm, R.E., 1973. Theory of gyrotrons with a non–fixed structure of the high frequency field. Radio Phys. Quantum Electron. 16, 474–480

Bratman, V.L., 1974. The starting regime for an MCR–monotron with a cavity having a low diffraction Q. Radio Phys. Quantum Electron. 17, 1181–1187

Bratman, V.L., Moiseev, M.A., 1975. Conditions for the self–excitation of a cyclotron resonance maser with a nonresonant electrodynamic system. Radio Phys. Quantum Electron. 18, 772–779

Bratman, V.L., Petelin, M.I., 1975. Optimizing the parameters of high power gyromonotrons with RF field of nonfixed structure. Radio Phys. Quantum Electron. 18, 1136–1140.

Bratman, V.L., Moiseev, M.A., Petelin, M.I., 1981a. Theory of gyrotrons with low–Q electromagnetic systems. From "Gyrotrons: collected papers", USSR Academy of Sciences, Insitute of Applied Physics, Gorki, 104

Bratman, V.L., Ginzburg, N.S., Nusinovich, G.S., Petelin, M.I., Strelkov, P.S., 1981b. Relativistic gyrotrons and cyclotron autoresonance masers. Int. J. Electronics 51, 541–567.

Bykov, Yu.V., Gol'denberg, A.L., 1975. Influence of resonator profile on the maximum power of a cyclotron resonance maser. Radio Phys. Quantum Electron. 18, 791–792

Bykov, Yu.V., Vlasov, S.N., Gol'denberg, A.L., Luchinin, A.G., Orlova, J.M., Petelin, M.I., Usov, V.G., Flyagin, V.A., Khizhnyak, V.I., 1981. Mode selection in high power gyrotrons. From "Gyrotrons: collected papers", USSR Academy of Sciences, Insitute of Applied Physics, Gorki, 153

Caplan, M., Lin, A.T., Chu, K.R., 1982. A study of the saturated output of a TE01 gyrotron using an electromagnetic finite size particle code. Int. J. Electronics 53, 659–671

Carmel, Y., Chu, K.R., Dialetis, D., Fliflet, A., Read, M.E., Kim, K.J., Arfin, B., Granatstein, V.L., 1982. Mode competition, suppression, and efficiency enhancement in overmoded gyrotron oscillators. Int. J. Infrared and Millimeter Waves 3, 645–665

Charbit, P., Herscovici, A., Mourier, G., 1981. A partly self consistent theory of the gyrotron. Int. J. Electronics 51, 303–330

Chu, K.R., 1978. Theory of the electron cyclotron maser interaction in a cavity at the harmonic frequencies. Phys. Fluids 21, 2354–2364.

Chu, K.R., Read, M.E., Ganguly, A.K., 1980. Methods of efficiency enhancement and scaling for gyrotron oscillators. IEEE Trans. Microwave Theory and Tech. MTT–28, 318–325.

Danly, B.G., Temkin, R.J., 1986. Generalized nonlinear harmonic gyrotron theory. Phys. Fluids 29, 561–567.

Dawson, J.M., 1983, Particle Simulation of Plasmas, Rev. Mod. Phys. 55, 403–447.

Derfler, H., Grant, T.J., Stone, D.S., 1982. Loaded Q's and field profiles of tapered axisymmetric gyrotron cavities. IEEE Trans Electron Dev. 29, 1917–1929.

Dialetis, D. Chu, K.R., 1983. Mode competition and stability analysis of the gyrotron oscillator. Infrared and Millimeter Waves 7, 537–581

Dumbrajs, O., Nusinovich, G.S., Pavelyev, A.B., 1987. Mode competition in a gyrotron with tapered magnetic field. Int. J. Electronics, 64, 137–145

Dumbrajs, O., Borie, E., 1988., A complex cavity with mode conversion for gyrotrons., Int. J. Electronics 65, 285–295.

Dumbrajs, O., Nusinovich, G.S., Pavelyev, A.B., 1990. Competition of modes resonant with arbitrary cyclotron harmonics in a gyrotron with nonfixed axial structure of the high frequency field. IEEE Trans Plasma Sci. 18, 301–305.

Edgcombe, C.J., 1983. A simple model for self–consistent calculation of the large signal behaviour of gyrotrons. Int. J. Electronics 55, 781–793

Felch, K., Bier, R., Craig, L.J., Huey, H., Ives, L., Jory, H., Lopez, N., Spang, S., 1986a. Achievements in the CW operation of 140 GHz gyrotrons. 11th Int. Conf. on Infrared and Millimeter Waves, Pisa. Conf. Digest pp. 43–45.

Felch, K., Bier, R., Craig, L.J., Huey, H., Ives, L., Jory, H., Lopez, N., Spang, S., 1986b. CW operation of a 140 GHz gyrotron. Int. J. Electronics 61, 701–714.

Felch, K., Huey, H., Jory, H., 1990. Gyrotrons for ECH Applications. J. Fusion Energy, 9, 59–75.

Feynman, R.P., Leighton, R.B., Sands, M., 1965. The Feynman Lectures in Physics, vol. III, Quantum Mechanics, Ch. 10, Addision–Wesley, Reading, MA.

Fliflet, A.W., Read, M.E., 1981. Use of weakly irregular waveguide theory to calculate eigenfrequencies, Q–values and RF field functions for gyrotron oscillators. Int. J. Electronics 51, 475–484.

Fliflet, A.W., Read, M.E., Chu, K.R., Seeley, R., 1982. A self–consistent field theory for gyrotron oscillators: application to a low Q gyromonotron. Int. J. Electronics 53, 505–521.

Fliflet, A.W., 1986. Linear and nonlinear theory of the Doppler shifted cyclotron resonance maser based on TE and TM waveguride modes. Int. J. Electronics 61, 1049–1080.

Fliflet, A.W., Lee, R.C., Read, M.E., 1988. Self–consistent field model for the complex cavity gyrotron . Int. J. Electronics 65, 273–283.

Fliflet, A.W., Hargreaves, T.A., Fischer, R.P., Manheimer, W.M., Sprangel, P., 1990. Review of quasi–optical gyrotron development. J. Fusion Energy, 9, 31–58.

Flyagin, V.A., Gaponov, A.V., Petelin, M.I., Yulpatov, V.K., 1977. The gyrotron. IEEE Trans. Microwave Theory and Tech. MTT–25, 514–521.

Flyagin, V.A., Gol'denberg, A.L.,Nusinovich, G.S., 1984. Powerful gyrotrons Infrared and Millimeter Waves, K. Button, ed. (Academic Press,New York), vol 11, 179–226.

Flyagin, V.A., Nusinovich, G.S., 1985. Powerful gyrotrons.for thermonuclear research. Infrared and Millimeter Waves, K. Button, ed. (Academic Press,New York), vol 13, 1–17.

Flyagin, V.A., Nusinovich, G.S., 1988. Gyrotron oscillators. Proceedings IEEE 76, 644–656.

Ganguly, A.K., Ahn, S., 1982. Self–consistent large signal theory of the gyrotron travelling wave amplifier. Int. J. Electronics 53, 641–658.

Ganguly, A.K., Chu, K.R., 1984. Limiting Current in Gyrotrons. Int. J. Infrared and Millimeter Waves 5, 103–121.

Gantenbein, G., Borie, E., 1990. Gyrotron with a tapered external magnetic field. Int. J. of Infrared and Millimeter Waves 11, 837–850.

Gaponov, A.V., Gol'denberg, A.L., Grigor'yev, D.P., Pankratova, T.B., Petelin, M.I., Flyagin, V.A., 1975. Experimental Study of centimeter band gyrotrons. Radio Phys. Quantum Electron. 18, 280

Gaponov, A.V., Flyagin, V.A., Gol'denberg, A.L., Nusinovich, G.S., Tsimring, Sh.E., Usov, V.G., Vlasov, S.N., 1981. Powerful millimeter wave gyrotrons. Int. J. Electronics 51, 277– 302.

Garin, G., Mourier, G., Teyssier, L., 1987. Symmetric and non–symmetric modes in high power generators for electron cyclotron resonance heating. 14th European Conference on Controlled Fusion and Plasma Heating, Madrid, 962.

Ginzburg, N.S., Zarnitsina, I.G. Nusinovich, G.S., 1981. Theory of relativistic cyclotron resonance maser amplifiers. Radio Phys. Quantum Electron. 24, 331–338.

Ginzburg, N.S., Zavolskii, N.A. Nusinovich, G.S., Sergeev, A.S., 1986. Self–Oscillation in uhf generators with diffraction radiation output Radio Phys. Quantum Electron. 29, 89–97.

Gold, S.H., Fliflet, A.W., Manheimer, W.M., Black, W.M., Granatstein, V.L., Kinkhead, A.K., Hardesty, D.L., Sucy, M., 1985. High voltage K_α–band gyrotron experiment. IEEE Trans. Plasma Sci. 13, 374–382.

Gold, S.H., Fliflet, A.W., Manheimer, W.M., McCowan, R.B., Black, W.M., Lee, R.C., Granatstein, V.L., Kinkhead, A.K., Hardesty, D.L., Sucy, M., 1987. High peak power K_α–band gyrotron oscillator experiment. Phys. Fluids 30, 2226–2234.

Hirschfield, J.L., Granatstein, V.L., 1977. The electron cyclotron maser– an historical survey. IEEE Trans. Microwave Theory and Tech. MTT–25, 522–527.

Halzen, F. and Martin, A.D., 1984. Quarks and Leptons, An intorductory course in modern particle physics, John Wiley and Sons, New York. Ch. 12,13.

Hockney, R.W., Eastwood, J.W., 1981. "Computer simulation using particles", McGraw–Hill Inc., Ch. 4.

James, F., and Roos, M., 1974, MINUIT long writeup, CERN Program Library, Programs D506, D516

Jackson, J.D., 1962. Classical Electrodynamics. John Wylie and Sons, New York.

Jödicke, B., 1989. Zur Modenrangigkeit von Hochleistungsgyrotrons mit rotationssymmetrischen Arbeitsmoden. KfK Report 4603.

Kleva, R.G., Antonsen, T.M., Levush, B., 1988. The effect of the time dependent self–consistent electrostatic field on gyrotron operation. Phys. Fluids 31, 375–386.

Kreischer, K.E., Temkin, R.J., 1980a. Linear theory of an electron cyclotron maser operating at the fundamental. Int. J. Infrared and Millimeter Waves 1, 195–233.

Kreischer, K.E., Temkin, R.J., 1980b. High frequency gyrotrons and their application to tokamak plasma heating. Infrared and Millimeter Waves 7, 377–485.

Kreischer, K.E., Schutkeker, J.B., Danly, B.G., Mulligan, W.J., Temkin, R.J., 1984a. High efficiency operation of a 140 GHz pulsed gyrotron. Int. J. Electronics 57, 835–850.

Kreischer, K.E., Danly, B.G., Woskoboinikov, P., Mulligan, W.J., Temkin, R.J., 1984b. Frequency pulling and bandwidth measurements of a 140 GHz pulsed gyrotron. Int. J. Electronics 57, 851–862.

Kreischer, K.E., Temkin, R.J., Fetterman, H.R., Mulligan, W.J., 1984c. Multimode oscillation and mode competition in high frequency gyrotrons IEEE Trans. Microwave Theory and Tech. MTT–32, 481.

Kreischer, K.E., Temkin, R.J., 1987. Single mode operation of a high power, step–tunable gyrotron. Phys. Rev. Lett. 59, 547–550.

Kreischer, K.E., Grimm, T.L., Guss, W.C., Möbius, A.W., Temkin, R.J., 1990. Experimental study of a high frequency megawatt gyrotron oscillator. Phys. Fluids B2, 640–646.

Kuraev, A.A., 1979. Theory and Optimization of high frequency electronic devices, (Minsk: Izd. Nauka i Tekhnika (in Russian)).

Levush, B., Bondeson, A., Manheimer, W.M., Ott, E., 1983. Theory of quasioptical gyrotrons and gyroklystrons operating at higher harmonics of the cyclotron frequency. Int. J. Electronics 54, 749–775.

Levush, B., Antonsen, T.M., 1990. Mode competition and control in high–power gyrotron oscillators, IEEE Trans. Plasma Sci. 18, 260–271.

Lin, A.T., Yang, Z.H., Chu, K.R., 1988. Particle simulation of a high–power gyrotron oscillator. IEEE Trans. Plasma Sci. 16, 129–134.

Lin, A.T., Lin, C.C., Yang, Z.H., Chu, K.R., Fliflet, A.W., Gold, S.H., 1988. Simulation of transient behavior in a pulse line driven gyrotron oscillator. IEEE Trans. Plasma Sci. 16, 135–141.

Lindsay, P.A., 1972. Cyclotron resonance interaction. Int. J. Electronics 33, 289–310.

Lindsay, P.A., Jones, R.M., Lumsden, R.J., 1984. Some observations on gyrotron interaction models. Int. J. Electronics 57, 915–951.

Luginsland, J. , 1985. Zur Berechnung inhomogener rotationssymmetrischer Gyrotronresonatoren. PhD Thesis, University of Aachen.

Lewin, L., 1975. Theory of Waveguides., Newnes–Butterworths, London.

Marcuvitz, N., 1951. Waveguide Handbook. MIT Radiation Laboratory Series, vol. 10., (McGraw–Hill, New York).

Malygin, S.A., Pavel'ev, V.G., Tsimring, Sh.E., 1983, Resonant Transformation of modes in oversize electrodynamic systems. Radio Phys. Quantum Electron. 26, 827–833.

Moiseev, M.A. and Nusinovich, G.S., 1974. Concerning the theory of multimode oscillation in a gyromonotron. Rad. Phys. Quant. Electron. 17, 1305–1311.

Neilson, J.M., Latham, P.E., Caplan, M., Lawson, W.G., 1989. Determination of the resonant frequencies in a complex cavity using the scattering matrix formalism. IEEE Trans. Microwave Theory and Tech. MTT–37, 1165–1169.

Nusinovich, G.S., 1981. Mode interaction in gyrotrons. Int. J. Electronics 51, 457–474 .

Nusinovich, G.S., 1986. Theory of mode interaction in the gyrotron. KfK Report 4111.

Nusinovich, G.S., Pavelyev, A.B., 1988. Mode competition in a gyrotron with an unfixed axial structure of an RF field. Preprint, USSR Academy of Sciences, Insitute of Applied Physics, Gorki

Pavelyev, V.G., Tsimring, Sh.E., Zapevalov, V.E., 1987. Complex cavities with mode conversion in gyrotrons. Int. J. Electronics 63, 379–391.

Petelin, M.I., 1974. On the theory of ultrarelativistic cyclotron self–resonance masers. Radio Phys. Quantum Electron. 17, 686–690

Petelin, M.I., 1981. Self–excitation of Oscillations in a gyrotron. From "Gyrotrons: collected papers", USSR Academy of Sciences, Insitute of Applied Physics, Gorki, 3

Rapoport, G.N., Nemark, A.K., Zhurakhovskij, V.A., 1967. Interaction of helical electron beams with the intense electromagnetic fields of cavities operating at harmonics of the cyclotron frequency. Radiotechnika i Elektronika 12, 633.

Riyopoulos, S., 1990. Multimode simulations without particles in the quasi–optical gyrotron. IEEE Trans. Plasma Sci. 18, 369–386.

Reiter, G., 1959. Generalized Telegraphist's equation for waveguides of varying cross section. Proc. Inst. elect. electron. Engrs. 106B, 54–57.

Salop, A., Caplan, M., 1986. Self–consistent large signal analysis of the gyroklystron. Int. J. Electronics 61, 1005–1024.

Scheid, F., 1968. Theory and Problems of Numerical Analysis (New York, McGraw Hill).

Schelkunoff, S.A., 1952. Generalized Telegraphist's equation for waveguides. Bell Syst. Tech. J., 31, 784–810.

Schelkunoff, S.A., 1955. Conversion of Maxwell's equations into generalized telegraphist's equations. Bell Syst. Tech. J., 34, 994–1043.

Solymar, L., 1959. Spurious mode generation in nonuniform waveguides. IEEE Trans. Microwave Theory and Tech. 7, 379–383.

Sprangle, P., Drobot, A.T., 1977. The linear and self–consistent nonlinear theory of the electron cyclotron maser instability. IEEE Trans. Microwave Theory and Tech. MTT–25, 528–544

Sprangle, P., Coffey, T. 1985. New high–power coherent radiation sources. Infrared and Millimeter Waves, K. Button, ed. (Academic Press,New York), vol 13, 1–17.

Sprangle, P., Vomvoridis, J.L., Manheimer, W.M., 1981. Theory of the quasioptical electron cyclotron maser. Phys. Rev. A23, 3127–3138.

Sporleder, F., Unger, H.G., 1979, Waveguide Tapers, Transitions and Couplers, Peter Peregrinus LTD.

Tran, T.M., Tran, M.Q., Alberti, S., Hogge, J.P.,., 1989. Prospects for high–power quasioptical gyrotrons operating in the millimeter wave range. IEEE Trans. Electron Devices 36, 1983–1990.

Vlasov, S.N., Zhislin, G.M., Orlova, I.M., Petelin, M.I., Rogacheva, G.G., 1969. Irregular waveguides as open resonators. Rad. Phys. Quant. Electron. 12, 972–978.

Vomvorides, J.L., 1982. Self–consistent nonlinear analysis of overmoded gyrotron oscillators. Int. J. of Infrared and Millimeter Waves 3, 339–366.

Weiland, T., 1984. On the numerical integration of Maxwell's equations and applications in the field of accelerator physics. DESY Preprint 84–006.

Xu, Cheng–he, Zhou, Le–zhu, 1983. Microwave open resonators in gyrotrons. Infrared and Millimeter Waves 10, 311–359.

List of Symbols

x_{mp} p'th Bessel zero for TE_{mp} modes, defined by $J'_m(x_{mp}) = 0$.
y_{mp} p'th Bessel zero for TM_{mp} modes, defined by $J_m(y_{mp}) = 0$.
$J_m(x)$ = Bessel function of order m .
$J'_m(x) = dJ_m(x)/dx$.
m = azimuthal index.
p = radial index.
ω = frequency of RF field, usually close to a harmonic of Ω_0/γ . $\omega/c = 2\pi/\lambda$.
m_e electron mass.
c speed of light in vacuum.
$Z_0 = \sqrt{\mu_0/\epsilon_0} \simeq 120\pi\ \Omega$. impedance of free space
e elementary charge.
R_0 = cavity radius. In gyrotrons, the wavelength of the outgoing radiation is related to R_0 by $\lambda \simeq 2\pi R_0/x_{mp}$.
R_e = radius of annular electron beam.
$k_{mp} = x_{mp}/R_0 \simeq 2\pi/\lambda$ is transverse wave number.

$\Omega_0 = eB/m_e$ electron cyclotron frequency
$r_L = \gamma v_\perp/\Omega_0$ Larmor radius

$\gamma = 1/\sqrt{1-\beta_\perp^2-\beta_z^2}$ relativistic factor

$\vec{u} = \gamma\vec{\beta} = \gamma\vec{v}/c$ normalized electron momentum.
$\alpha = v_\perp/v_z$ velocity ratio
Q quality factor.
Q_D diffractive quality factor.
Q_Ω ohmic quality factor.